

# QGP Physics from Attractor Perturbations

Xin An<sup>1,\*</sup> and Michał Spaliński<sup>1,2,†</sup>

<sup>1</sup>*National Centre for Nuclear Research, 02-093 Warsaw, Poland*

<sup>2</sup>*Physics Department, University of Białystok, 15-245 Białystok, Poland*

The strong longitudinal expansion characteristic of heavy-ion collisions leads to universal attractor behavior of the resulting drop of quark-gluon plasma (QGP) already at very early times. Assuming approximate boost invariance and neglecting transverse expansion at the initial time, we incorporate subsequent transverse dynamics of this system by linearizing the Mueller-Israel-Stewart theory around the transversely homogeneous attractor. The result is a system of coupled ordinary differential equations which describes the proper-time evolution of Fourier modes encoding the transverse structure of the initial energy deposition. The late-time asymptotic behavior of these solutions is described by transseries which make manifest the stability of the attractor against transverse perturbations. In this framework, information about the structure of the plasma in the transverse plane resides mostly in exponentially suppressed corrections to evolution along the attractor, which are not yet negligible at freeze-out. These findings also suggest a simple numerical approach to QGP dynamics using a finite number of Fourier modes. Physical observables can be expressed in terms of the asymptotic data evaluated at freeze-out. We demonstrate the efficacy of this approach by calculating the final multiplicity distributions and collective flow coefficients.

## I. INTRODUCTION

Quark-gluon plasma (QGP) is created in heavy-ion collision experiments in highly anisotropic, nonequilibrium states. Many features of the subsequent evolution are successfully described by models formulated in the language of fluid dynamics, which are applied long before local equilibrium is established. This implies a vast reduction in the number of degrees of freedom at the earliest moments following the collision. A possible explanation of this follows from a key kinematical feature of heavy-ion collisions: the dominant longitudinal expansion at the prehydrodynamic stages of evolution. An idealization of this situation assumes boost invariance along the collision axis and neglects the transverse dynamics [1]. It has been shown in a number of models that in such circumstances an early-time, far-from-equilibrium attractor governs the dynamics until the QGP drop approaches a state amenable to a hydrodynamic description with small gradients [2–5]. Within such a picture, the information about the initial state is contained in a single scale which characterizes the particular attractor background, up to corrections which are exponentially suppressed – and thus effectively lost – at asymptotically late times. Of course, what actually happens

\* [xin.an@ncbj.gov.pl](mailto:xin.an@ncbj.gov.pl)

† [michal.spalinski@ncbj.gov.pl](mailto:michal.spalinski@ncbj.gov.pl)

in heavy-ion collision experiments is that the system does not survive until such asymptotically late times, because as the effective local temperature drops, the cooling QGP is converted into a stream of hadrons which source the multitude of particles registered in detectors. This results in a wealth of information which reflects the structure of the initial state primarily encoded in the dynamics in the plane transverse to the collision axis. Our goal is to extend the Bjorken model so as to account for transverse dynamics in a way which still allows for some analytic insights. We will show that within such a description, essentially all of the information about the initial state encoded in the spectra of outgoing hadrons resides in exponentially suppressed terms which are not yet negligibly small at the time of freeze-out. While this picture must still be viewed as a toy model, it provides a manageable playground which extends the range of phenomena which can be addressed, well beyond the scope of the original Bjorken model.

We focus on a version of the theory originally due to Müller [6] and Israel and Stewart [7, 8] (MIS) which can be viewed as a possible “UV-completion” of Navier-Stokes (NS) theory of hydrodynamics. It describes the universal hydrodynamic regime which emerges at late times, but also includes a nonhydrodynamic sector which is necessary for causality [9] and provides a very simple model of the dynamics at earlier times (see e.g. [10–12]). Our analysis retains the assumption of longitudinal boost invariance, and accounts for the transverse dynamics at the level of linearization around the boost-invariant and transversely homogeneous attractor. At the initial time the expansion is assumed to be purely longitudinal, but the dynamics induces a build-up of transverse flow which expresses the structure of the energy density at the initial time. The linearized fields capture all the dependence of the fireball on the transverse coordinates, and are conveniently analyzed in Fourier space. Under this assumption, the full MIS equations reduce to a system of coupled ordinary differential equations for a set of modes parametrized by the transverse wave vector.

The asymptotic solutions of this system at large proper time can be studied analytically. Since the background is homogeneous in the transverse plane, its dynamics carries no information about the transverse structure of the initial state. In fact, the only information about the initial state carried by the background solution which is not exponentially suppressed at late times is the overall energy scale (see e.g. [11]). All the information about the transverse structure of the initial energy deposition is encoded in the evolution of the perturbations. We find that these perturbations of the background are exponentially damped (apart from zero modes) and show that essentially all physical observables are determined by these corrections. Thus, the physics of QGP flow in heavy-ion collisions provides an example of a very nontrivial dynamical system where the exponentially damped corrections to asymptotic results are not just non-negligible, but in fact contain almost all of the physically relevant information. One can usefully distinguish three phases of evolution: the expansion-dominated initial stage whose course depends weakly on the parameters of the theory, the asymptotic near-equilibrium hydrodynamic stage where all information about the transverse dynamics is exponentially suppressed and effectively undetectable, and the intermediate stage

where the transseries corrections are not yet negligible and carry almost all the information about the initial state. They also reflect the nonhydrodynamic content of the theory.

Linearized perturbations around relativistic hydrodynamic flows were extensively investigated some years ago in the context of Navier-Stokes theory (see, e.g., Ref. [13]). It has since been recognized that in the context of heavy-ion physics one needs models which describe equilibration at times when the nonhydrodynamic sector still plays a crucial role, which manifests itself through the form of the attractor and its perturbations. The simplest of such models is the MIS theory considered here (see also, e.g., Ref. [14]). More elaborate models could of course be considered along the same lines, by identifying the transversely homogeneous attractor locus and accounting for transverse dynamics at the linear level.

This paper is organized as follows. In Sec. II we present the variant of MIS theory which we adopt to illustrate the approach outlined above and we describe the asymptotics of the background solutions at early as well as late times. Especially important are solutions on the attractor locus, which we analyze in greater detail than can be found in the existing literature. Sec. III introduces perturbations around the attractor, which bring in dependence on the transverse coordinates. The equations for linearized perturbations are given and their late-time asymptotics are studied and found to agree very well with numerical calculations already at moderate times. One result of this asymptotic analysis is the precise form of the suppression of short wavelength modes. We use this fact to implement a simple numerical scheme whereby a finite set of modes is evolved and used to reconstruct the spacetime evolution of an initial QGP drop. In Sec. IV we demonstrate that our approach qualitatively captures effects of the transverse collective expansion, such as elliptic flow. This is somewhat reminiscent of the effectiveness of the close limit in studies of black hole collisions [15]. In Sec. V we offer a summary of our findings along with some remarks on how the approach presented here might be developed further.

## II. MIS THEORY AND THE ATTRACTOR BACKGROUND

The MIS theory is expressed in terms of the classical fields  $\mathcal{E}$  (the energy density),  $u^\mu$  (the flow velocity) and  $\pi^{\mu\nu}$  (the shear-stress tensor). They satisfy the following set of partial differential equations

$$u \cdot \nabla \mathcal{E} = -(\mathcal{E} + p) \nabla \cdot u + u^\nu \nabla^\mu \pi_{\mu\nu}, \quad (1a)$$

$$(\mathcal{E} + p) u \cdot \nabla u_\mu = -\Delta_{\mu\nu} \nabla^\nu p - \Delta_{\mu\nu} \nabla_\lambda \pi^{\nu\lambda}, \quad (1b)$$

$$\Delta_{\mu\alpha} \Delta_{\nu\beta} u \cdot \nabla \pi^{\alpha\beta} = - \left( 1 + \frac{4}{3} \tau_\pi \nabla \cdot u \right) \pi_{\mu\nu} - 2\eta \sigma_{\mu\nu}, \quad (1c)$$

where  $\nabla_\mu$  is the covariant derivative,  $\Delta_{\mu\nu} \equiv g_{\mu\nu} + u_\mu u_\nu$  is the transverse projector,  $\sigma_{\mu\nu} = \frac{1}{2}\Delta_{\mu\alpha}\Delta_{\nu\beta}(\nabla^\alpha u^\beta + \nabla^\beta u^\alpha - \frac{2}{3}\Delta^{\alpha\beta}\nabla \cdot u)$  is the shear tensor,  $\eta$  is the shear viscosity and  $\tau_\pi$  is the relaxation time for  $\pi_{\mu\nu}$ . Throughout this paper we assume an equation of state and transport coefficients dictated by conformal invariance:

$$\mathcal{E} = \frac{1}{3}p = C_e T^4, \quad \eta = \frac{4}{3}C_e C_\eta T^3, \quad \tau_\pi = C_\tau T^{-1}, \quad (2)$$

where  $C_e$ ,  $C_\eta$ , and  $C_\tau$  are dimensionless, constant transport coefficients (see e.g. [11]) and  $T$  is the effective temperature. For  $\mathcal{N} = 4$  supersymmetric Yang-Mills theory we have  $C_e = 8\pi^2/15$ ,  $C_\eta = 1/4\pi$ ,  $C_\tau = (2 - \ln 2)/2\pi$  [16]. These values often serve as a point of reference, and we have adopted them in our numerical calculations.

The basic physical picture we adopt is that of the Bjorken model [1]: at sufficiently high energies, in the first approximation, the system exhibits boost invariance in the longitudinal direction and homogeneity in the transverse directions (perpendicular to the collision axis  $z$ ). We will refer to this approximate description as the background; perturbations dependent on the transverse coordinates will subsequently be treated at the linearized level. Under these assumptions, the energy-momentum tensor of the conformal MIS theory can be parametrized in terms of only two functions of proper time  $\tau = \sqrt{t^2 - z^2}$ : the effective temperature  $T(\tau)$ , and the pressure anisotropy  $\mathcal{A}(\tau) = 9\pi_i^i/2\mathcal{E}$ , where  $i = 1, 2$  labels the transverse coordinates (for details see [12]). Eqs. (1) then reduce to

$$\tau \partial_\tau \ln T(\tau) = -\frac{1}{3} + \frac{1}{18}\mathcal{A}(\tau), \quad (3a)$$

$$\tau \partial_\tau \mathcal{A}(\tau) = 8\alpha^2 - \frac{\tau T(\tau)}{C_\tau} \mathcal{A}(\tau) - \frac{2}{9}\mathcal{A}^2(\tau), \quad (3b)$$

where

$$\alpha \equiv \sqrt{\frac{C_\eta}{C_\tau}}. \quad (4)$$

In the NS limit ( $C_\tau \rightarrow 0$ ), Eq. (3b) becomes algebraic and one finds the well-known solutions

$$T_{\text{NS}}(\tau) = \Lambda(\Lambda\tau)^{-\frac{1}{3}} \left( 1 - \frac{2C_\eta}{3}(\Lambda\tau)^{-\frac{2}{3}} \right), \quad (5a)$$

$$\mathcal{A}_{\text{NS}}(\tau) = \frac{8C_\eta}{\tau T(\tau)} \sim 8C_\eta(\Lambda\tau)^{-\frac{2}{3}} \left( 1 + \sum_{n=1}^{\infty} \left( \frac{2C_\eta}{3} \right)^n (\Lambda\tau)^{-\frac{2n}{3}} \right), \quad (5b)$$

where  $\Lambda$  is an integration constant with the dimension of energy.

General solutions of Eqs. (3) are not available in closed form and can only be found in certain regimes. However, there are some special (and exact) solutions which are completely independent of any integration constants:  $T = 0$ ,  $\mathcal{A} = \pm 6\alpha$  and  $T = \frac{2(4-\alpha^2)}{3C_\tau}$ ,  $\mathcal{A} = -12$ . We regard these solutions

as unphysical, since they require fine-tuning of the initial conditions. To understand physically interesting solutions, we will resort to approximations valid at small or large proper times.

At early times Eqs. (3) admits two special families of solutions which can be characterized by having a finite value of the pressure anisotropy at  $\tau = 0$ :

$$T_{\pm}(\tau) \sim \mu(\mu\tau)^{-\frac{1}{3}(1\mp\alpha)} \left( 1 \pm \sum_{n=1}^{\infty} t_n^{(0)} (\mu\tau)^{\frac{n}{3}(2\pm\alpha)} \right), \quad (6a)$$

$$\mathcal{A}_{\pm}(\tau) \sim \pm 6\alpha \left( 1 \pm \sum_{n=1}^{\infty} a_n^{(0)} (\mu\tau)^{\frac{n}{3}(2\pm\alpha)} \right), \quad (6b)$$

where  $\mu$  is an integration constant. The early-time series coefficients  $t_n^{(0)}$  and  $a_n^{(0)}$  are rational functions of the transport coefficients and the first few are given by

$$t_1^{(0)} = -\frac{3\alpha}{C_{\tau}(2+\alpha)(2+9\alpha)}, \quad t_2^{(0)} = \frac{9\alpha(2+9\alpha+12\alpha^2)}{2C_{\tau}^2(2+\alpha)^2(2+5\alpha)(2+9\alpha)^2}, \quad \dots \quad (7a)$$

$$a_1^{(0)} = \frac{18\alpha}{C_{\tau}(2+9\alpha)}, \quad a_2^{(0)} = \frac{54\alpha(2+7\alpha+7\alpha^2)}{C_{\tau}^2(2+\alpha)(2+5\alpha)(2+9\alpha)^2}, \quad \dots \quad (7b)$$

The power series appearing in Eqs. (6) have a finite radius of convergence. The upper sign in Eqs. (6) defines the class of attractor solutions labeled by  $\mu$ . It is easy to check that all these solutions are mapped to the universal attractor introduced in Ref. [2] (see also the reviews [11, 12, 17, 18]). The solutions with the lower sign are mapped to the ‘‘repulsor’’ solution noted in the original approach of Ref. [2] (see also the recent Ref. [19]).

There are also ‘‘generic’’ solutions, characterized by a pressure anisotropy which diverges at early times. These solutions approach the attractor already in the far from equilibrium regime. To understand this, it is important to keep in mind that since Eqs. (3) are nonautonomous, the full phase space of solutions is three-dimensional and can be naturally parametrized by  $(\tau, T, \tau T')$  [20] (see also Refs. [12, 18]). The attractor is a two-dimensional surface in this full phase space. In any constant proper-time slice of the phase space,  $\mu$  is a parameter that labels points along the attractor curve on that slice. The generic solutions viewed on a sequence of such phase-space slices at increasing values of  $\tau$  gravitate toward this locus, as a consequence of the fast longitudinal expansion at early times. This is illustrated in Fig. 1.

At late times, we expect the system to approach equilibrium in a way consistent with the original insights of Bjorken [1]. In that regime, solutions to Eqs. (3) can be represented in the form

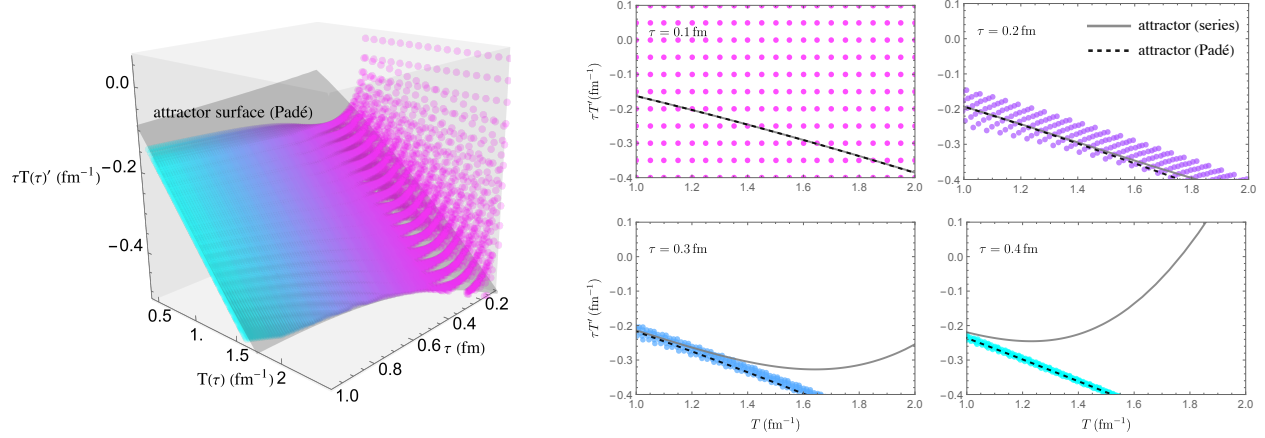


FIG. 1. The left panel shows the early-time attractor in the 3D phase space  $(\tau, T, \tau T')$  with uniformly distributed initial conditions (points) at  $\tau = 0.1$  fm. The 2D attractor surface is obtained using Padé approximation of the series in Eqs. (6). The right panel are the snapshots of the 3D plot at different times, where the solid and dashed line represents the series solution and its Padé approximant respectively.

of transseries

$$T(\tau) \sim \Lambda \left[ (\Lambda\tau)^{-\frac{1}{3}} \left( 1 + \sum_{n=1}^{\infty} t_n^{(\infty)} (\Lambda\tau)^{-\frac{2n}{3}} \right) + C_{\infty} (\Lambda\tau)^{\frac{2}{3}\alpha^2 - 1} e^{-\frac{3}{2C_{\tau}} (\Lambda\tau)^{\frac{2}{3}}} \left( 1 + \mathcal{O}((\Lambda\tau)^{-\frac{2}{3}}) \right) + \dots \right], \quad (8a)$$

$$\mathcal{A}(\tau) \sim 8C_{\eta} (\Lambda\tau)^{-\frac{2}{3}} \left( 1 + \sum_{n=1}^{\infty} a_n^{(\infty)} (\Lambda\tau)^{-\frac{2n}{3}} \right) + C'_{\infty} (\Lambda\tau)^{-\frac{2}{3}\alpha^2} e^{-\frac{3}{2C_{\tau}} (\Lambda\tau)^{\frac{2}{3}}} \left( 1 + \mathcal{O}((\Lambda\tau)^{-\frac{2}{3}}) \right) + \dots \quad (8b)$$

These are of the form of an asymptotic power series augmented by an infinite set of exponential transseries contributions, of which only the leading one is displayed above. The first few coefficients of the late-time series  $t_n^{(\infty)}$  and  $a_n^{(\infty)}$  are given by

$$t_1^{(\infty)} = -\frac{2C_{\tau}\alpha^2}{3}, \quad t_2^{(\infty)} = -\frac{2C_{\tau}^2\alpha^2}{9}, \quad \dots \quad (9a)$$

$$a_1^{(\infty)} = \frac{2C_{\tau}}{3}(1 + \alpha^2), \quad a_2^{(\infty)} = \frac{2C_{\tau}^2}{9}(4 - \alpha^2 + 2\alpha^4), \quad \dots \quad (9b)$$

The power series appearing in Eqs. (8) have a vanishing radius of convergence and are best interpreted in the sense of asymptotic analysis – through optimal truncation or by Borel summation (see, e.g. Refs. [19, 21]). Note that in the limit  $C_{\tau} \rightarrow 0$  the leading and next-to-leading terms in Eqs. (8) reduce to their NS form, given in Eq. (5), upon substituting the coefficients in Eqs. (9).

Initial conditions are mapped to the dimensionful scale  $\Lambda$  and the dimensionless integration constant  $C_{\infty}$  (the constant  $C'_{\infty}$  is not independent). Given a specific solution, the corresponding values of  $\Lambda$  and  $C_{\infty}$  can be obtained by fitting the leading terms in Eq. (8) at late-times. For initial conditions relevant to heavy-ion physics one typically finds  $\Lambda \approx \mathcal{O}(1) \text{ fm}^{-1}$ .

The description of the attractor presented above differs from the original formulation of Ref. [2] in that it uses proper time as the evolution parameter, rather than the dimensionless evolution variable  $\tau T$ . This is natural when the dynamic system possesses scales in addition to temperature, as will be discussed in Sec. III. It is also worth emphasizing that while the attractor is often referred to as hydrodynamic, it coincides with hydrodynamics only at late times. At earlier, pre-hydrodynamic, times it depends on the nonhydrodynamic content of the microscopic theory under consideration.

### III. THE TRANSVERSE PERTURBATIONS

In the previous section, we discussed the Bjorken background solution, which is an idealized description where all the fields are homogeneous in the transverse plane. While this idealization provides a useful first approximation for modeling heavy-ion collisions at sufficiently high energies, it cannot account for physical observables which depend on the structure of the plasma in the transverse plane. In this section, we relax the transverse homogeneity condition by considering additional fields which aim to model the transverse dynamics. These additional fields arise as perturbations of the fully nonlinear hydrodynamic equations (1) around the attractor background.

#### A. The linearized equations

We will look for solutions that can be approximated by the boost-invariant and translation-invariant background solution discussed in Sec. II and a perturbation depending also on the transverse coordinates:

$$T(\tau, \mathbf{x}) = T(\tau) + \delta T(\tau, \mathbf{x}), \quad u^\mu(\tau, \mathbf{x}) = u^\mu + \delta u^\mu(\tau, \mathbf{x}), \quad \pi^{\mu\nu}(\tau, \mathbf{x}) = \pi^{\mu\nu}(\tau) + \delta \pi^{\mu\nu}(\tau, \mathbf{x}), \quad (10)$$

where  $\mathbf{x} = (x_1, x_2)$  labels the coordinates of the transverse plane. We shall always retain the argument  $\mathbf{x}$  of the above quantities to distinguish the full ones from the background, which depends only on  $\tau$  (and, as the only argument, is often suppressed). The background fields  $T$  and  $\pi^{\mu\nu}$  are taken to be on the attractor locus defined in Sec. II, and  $u^\mu = (-1, \mathbf{0}, 0)$ . Due to the assumed symmetries and the transversality condition  $u^\mu \pi_{\mu\nu} = 0$ , the shear-stress tensor has only one independent background component (i.e.,  $\pi^{11} = \pi^{22}$ ) and three independent perturbation components (i.e.,  $\delta\pi^{11}, \delta\pi^{22}, \delta\pi^{12}$ ) that couple to the perturbation of hydrodynamic fields  $\delta T$  and  $\delta \mathbf{u}$ . We also put  $\delta\pi^{i\eta} = 0$ , which is consistent due to  $\delta u^\eta = 0$ .

The perturbation fields can also be normalized by the background energy scale  $T(\tau)$ , i.e.,

$$\delta\hat{T}(\tau, \mathbf{x}) = \frac{\delta T(\tau, \mathbf{x})}{T(\tau)}, \quad \delta\hat{\pi}_{ij}(\tau, \mathbf{x}) = \frac{\delta\pi_{ij}(\tau, \mathbf{x})}{C_e T(\tau)^4}, \quad (11)$$

such that all six perturbation fields, collectively denoted by  $\hat{\phi}(\tau, \mathbf{x}) = (\delta\hat{T}, \delta u_1, \delta u_2, \delta\hat{\pi}_{12}, \delta\hat{\pi}_{11}, \delta\hat{\pi}_{22})$ , are dimensionless. Since the background is independent of the transverse coordinates, it is also natural and convenient to introduce the Fourier transforms just for the perturbations:

$$\hat{\phi}(\tau, \mathbf{x}) = \int \frac{d^2k}{(2\pi)^2} e^{i\mathbf{k}\cdot\mathbf{x}} \hat{\phi}(\tau, \mathbf{k}), \quad (12)$$

where we retain the argument  $\mathbf{x}$  or  $\mathbf{k}$  to distinguish perturbation fields  $\hat{\phi}$  in different Fourier spaces.

Linearization of the full MIS equations (1) around an attractor solution leads to a system of six linear partial differential equations for the perturbations. For each value of  $\mathbf{k}$  the set of six modes  $\hat{\phi}(\tau, \mathbf{k}) \equiv (\delta\hat{T}, \delta u_1, \delta u_2, \delta\hat{\pi}_{12}, \delta\hat{\pi}_{11}, \delta\hat{\pi}_{22})$  satisfies a linear system of evolution equations which can be explicitly written as

$$4 \left( \tau \partial_\tau + \frac{2\mathcal{A}}{9} \right) \delta\hat{T} + \frac{(12 + \mathcal{A})}{9} i\tau k_i \delta u^i - \delta\hat{\pi}_i^i = 0, \quad (13a)$$

$$\frac{4}{3} i\tau k_i \delta\hat{T} + \frac{1}{9} \left[ (12 + \mathcal{A})\tau \partial_\tau - 4 + 8\alpha^2 + \left( \frac{7}{3} - w \right) \mathcal{A} \right] \delta u_i + i\tau k^j \delta\hat{\pi}_{ij} = 0, \quad (13b)$$

$$\begin{aligned} \frac{1}{9} (w\mathcal{A} - 32\alpha^2) \delta_{ij} \delta\hat{T} + \frac{4}{27} i\tau [(\mathcal{A} - 6\alpha^2) \delta_{ij} k_\ell + 9\alpha^2 (\delta_{i\ell} k_j + \delta_{j\ell} k_i)] \delta u^\ell \\ + \left( \tau \partial_\tau + w + \frac{2\mathcal{A}}{9} \right) \delta\hat{\pi}_{ij} = 0, \end{aligned} \quad (13c)$$

where  $w(\tau) = \tau T(\tau)/C_\tau$ . Since modes with different  $\mathbf{k}$  are decoupled at the linearized level, we omit the arguments  $\tau$  and  $\mathbf{k}$  unless needed.

## B. Numerical evolution of the modes

It is straightforward to numerically solve the system of ODEs given in Eqs. (13) together with Eqs. (3) for any given wave vector  $\mathbf{k}$ . To do this we need to choose a background solution  $T(\tau), \mathcal{A}(\tau)$  and initial conditions for the modes. In practice, one would take an initial condition for all the hydrodynamic fields taken from some model of the initial state and represent them as a homogeneous background plus a perturbation as in Eqs. (13). The initial values for the modes can then be obtained from this by calculating the Fourier transform of the spacetime perturbations with respect to the transverse coordinates. The Fourier modes can then be evolved by solving the system Eqs. (13) for each mode. To reconstruct the spacetime fields one then needs to invert the Fourier transform. In practice this has to be done numerically by discretizing the transverse space (and the corresponding space of wave vectors). We will discuss how this can be done in more detail in Sec. IV, but in this section we will only consider how the dynamics of the Fourier modes depends on the wave vectors  $\mathbf{k}$ .

The results of such a numerical calculation are shown in Fig. 2. The most obvious feature of the



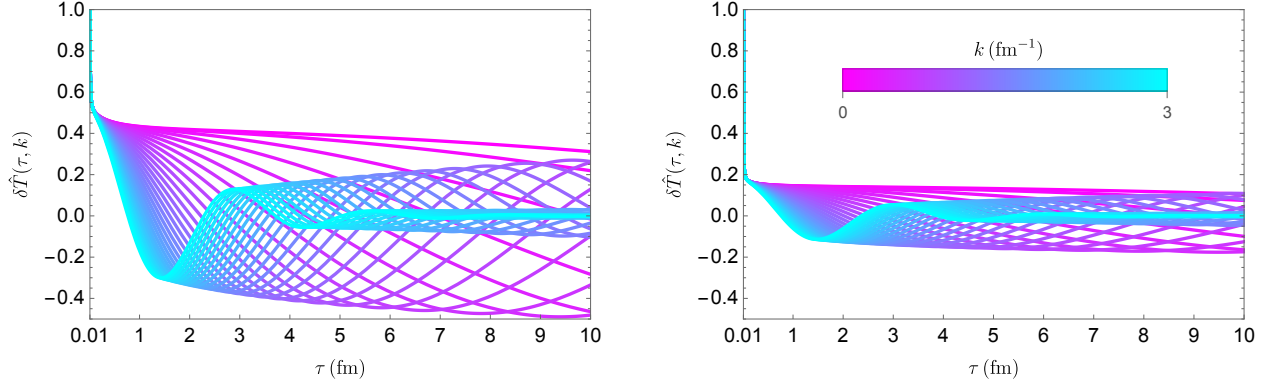


FIG. 2. Evolution of Fourier modes with various values of  $k$  between  $0 - 3 \text{ fm}^{-1}$ , with the background initially resided on the attractor,  $\mathcal{A}(0) \simeq 6\alpha$  (left) and off it,  $\mathcal{A}(0) \simeq 30\alpha$  (right), with initial values of  $\delta\hat{T}$  fixed to 1 for different values of  $k$ .

results is the fact that modes with higher  $k$  are damped more strongly than modes with low  $k$ , as illustrated in the left panel of Fig. 2. The origin of this phenomenon can be understood analytically, as will be discussed in Sec. III C. Moreover, one can also see that the perturbations starting away from the attractor are damped more significantly than perturbations starting on the attractor, as illustrated in the right panel of Fig. 2. This suggests the stability of the linearization around the attractor background and reveals its dominant role in the presence of transverse dynamics. We will refine this statement based on analytic results presented in Sec. III C.

### C. Late-time behavior of perturbations

The main goal of this section is to understand analytically the main features of the numerical solutions of the mode equations Eqs. (13) described in Sec. III A, especially the stability of the Bjorken attractor background. To this end, we will study the late proper-time behavior of the modes  $\hat{\phi}(\tau, \mathbf{k})$ . The set of six ODEs describing the evolution of the modes  $\hat{\phi}$  can be analyzed by standard asymptotic methods, although the complexity of this problem makes the calculation technically nontrivial. In doing this it is important to recognize that the case when  $\mathbf{k} = 0$  must be treated separately, do to the presence of products such as  $\mathbf{k}\tau$  in the mode evolution equations. We will first consider the case when  $\mathbf{k} \neq 0$ , returning to the issue of the zero-modes at the end of this section.

For the purpose of calculating the asymptotics it is convenient to introduce the transverse divergence  $\delta\theta(\tau, \mathbf{x}) \equiv \partial_i \delta u^i$  and longitudinal vorticity  $\delta\omega(\tau, \mathbf{x}) \equiv \epsilon_{ij} \partial^i \delta u^j$  where  $\epsilon_{ij}$  is the Levi-Civita symbol. In  $\mathbf{k}$  space we will use the following dimensionless quantities, normalized by  $k \equiv |\mathbf{k}|$ :

$$\delta\hat{\theta}(\tau, \mathbf{k}) = \frac{\delta\theta(\tau, \mathbf{k})}{k} = i\hat{k}_i \delta u^i(\tau, \mathbf{k}), \quad \delta\hat{\omega}(\tau, \mathbf{k}) = \frac{\delta\omega(\tau, \mathbf{k})}{k} = i\epsilon_{ij} \hat{k}^i \delta u^j(\tau, \mathbf{k}), \quad (14)$$

where  $\hat{k}_i \equiv k_i/k$ . For such a choice of variables, the linear system of evolution equations reads

$$4 \left( \tau \partial_\tau + \frac{2\mathcal{A}}{9} \right) \delta \hat{T} + \frac{(12 + \mathcal{A})}{9} \tau k \delta \hat{\theta} - \delta \hat{\pi}_i^i = 0, \quad (15a)$$

$$-\frac{4}{3} k^2 \delta \hat{T} + \frac{1}{9\tau} \left[ (12 + \mathcal{A}) \tau \partial_\tau - 4 + 8\alpha^2 + \left( \frac{7}{3} - w \right) \mathcal{A} \right] k \delta \hat{\theta} - k_i k_j \delta \hat{\pi}^{ij} = 0, \quad (15b)$$

$$\frac{1}{9\tau} \left[ (12 + \mathcal{A}) \tau \partial_\tau - 4 + 8\alpha^2 + \left( \frac{7}{3} - w \right) \mathcal{A} \right] k \delta \hat{\omega} - \epsilon_{ij} k^j k^\ell \delta \hat{\pi}_\ell^i = 0, \quad (15c)$$

$$\begin{aligned} & \frac{1}{9} (w\mathcal{A} - 32\alpha^2) \delta_{ij} \delta \hat{T} + \frac{4\tau}{27k} [18\alpha^2 k_i k_j + (\mathcal{A} - 6\alpha^2) k^2 \delta_{ij}] \delta \hat{\theta} \\ & - \frac{4\alpha^2 (k_i \epsilon_{j\ell} + k_j \epsilon_{i\ell}) k^\ell \tau}{3k} \delta \hat{\omega} + \left( \tau \partial_\tau + w + \frac{2\mathcal{A}}{9} \right) \delta \hat{\pi}_{ij} = 0. \end{aligned} \quad (15d)$$

In these equations the quantities  $T$  and  $\mathcal{A}$  refer to the background solutions, expanded as in Eq. (8). As discussed earlier, this late-time asymptotics of the background depends on the scale  $\Lambda$  which is determined by the initial conditions of the background. This scale will therefore appear also in the asymptotics of the perturbations.

At this juncture, one way to proceed is to rewrite this system in terms of higher-order ODEs; remarkably, it can be written as a set of three second-order ODEs for  $\delta \hat{T}$ ,  $\delta \hat{\theta}$ ,  $\delta \hat{\omega}$  – they are given in Appendix A. Two of these equations couple  $\delta \hat{T}$  and  $\delta \hat{\theta}$ , while the third involves  $\delta \hat{\omega}$  alone. The two coupled equations can be combined into a fourth-order ODE for  $\delta \hat{T}$ , whose asymptotic behavior can be studied by standard methods (see, e.g., Ref [22]). This is in principle straightforward, but is somewhat challenging in practice due to the complexity of the coefficients which appear in this equation. Alternatively, one can analyze the system of six first-order ODEs directly using the methods developed in Ref. [23]. Both approaches gives rise to the same late-time asymptotic solutions whose *leading* terms take the form:

$$\delta \hat{T} \sim \sum_{i=1}^4 C_i (\Lambda \tau)^{\beta_i} e^{-i\omega_i \tau - A_i (\Lambda \tau)^{\frac{2}{3}}} \left( 1 + \mathcal{O}((\Lambda \tau)^{-\frac{2}{3}}) \right), \quad (16a)$$

$$\delta \hat{\theta} \sim \sum_{i=1}^4 C'_i (\Lambda \tau)^{\beta'_i} e^{-i\omega_i \tau - A_i (\Lambda \tau)^{\frac{2}{3}}} \left( 1 + \mathcal{O}((\Lambda \tau)^{-\frac{2}{3}}) \right), \quad (16b)$$

$$\delta \hat{\omega} \sim \sum_{i=5}^6 C_i (\Lambda \tau)^{\beta_i} e^{-i\omega_i \tau - A_i (\Lambda \tau)^{\frac{2}{3}}} \left( 1 + \mathcal{O}((\Lambda \tau)^{-\frac{2}{3}}) \right). \quad (16c)$$

The initial conditions are accounted for by the amplitudes  $C_1, \dots, C_6$  and  $C'_1, \dots, C'_4$ . The primed integration constants are related to the unprimed ones by the relations

$$C'_1 = 3ic_\infty C_1, \quad C'_2 = -3ic_\infty C_2, \quad C'_3 = -\frac{(1 - 3\alpha^2)\Lambda}{2\alpha^2 k} C_3, \quad C'_4 = \frac{\Lambda}{c_\infty^2 C_\tau k} C_4, \quad (17)$$

so that only the unprimed integration constants  $C_1, \dots, C_6$  are independent. Recall also that each

of the perturbations appearing above depends on the wave vector  $\mathbf{k}$ , and so do the coefficients  $C_1, \dots, C_6$ .

The remaining quantities appearing in Eqs. (16) above are determined in terms of the parameters of the theory and do not depend on the initial state. The parameters appearing in the exponentials are given by

$$\begin{aligned} A_1 = A_2 &= \frac{\alpha^2}{C_\tau c_\infty^2}, & A_3 &= \frac{3}{2C_\tau}, & A_4 &= \frac{1}{2C_\tau c_\infty^2}, & A_5 = A_6 &= \frac{3}{4C_\tau}, \\ \omega_1 = -\omega_2 &= c_\infty k \left[ 1 + \frac{2\alpha^2}{3c_\infty^2} \left( 2C_\tau(1 - \alpha^2) - \frac{(1 + \alpha^2)\Lambda^2}{C_\tau^2 c_\infty^4 k^2} \right) (\Lambda\tau)^{-\frac{2}{3}} \right], & \omega_3 = \omega_4 &= 0, \\ \omega_5 = -\omega_6 &= \alpha k \left[ 1 - \left( C_\tau \alpha^2 + \frac{3\Lambda^2}{8C_\tau^2 \alpha^2 k^2} \right) (\Lambda\tau)^{-\frac{2}{3}} \right], \end{aligned} \quad (18)$$

where

$$c_\infty = \sqrt{\frac{1}{3}(1 + 4\alpha^2)} \quad (19)$$

is the asymptotic speed of sound of MIS theory, which remains subluminal as long as  $\alpha^2 < 1/2$  (or  $C_\tau > 2C_\eta$ ). The constant coefficients  $A_i$  are the leading contributions to eigenvalues of the coupled linear equations describing perturbations around the attractor. They are real, positive and independent of the wave vectors  $k$ , implying stability of the attractor against transverse perturbations regardless of their amplitudes. Note that the quantities  $\omega_1 = -\omega_2$  and  $\omega_5 = -\omega_6$  are actually functions of  $\tau$ , which also have a nontrivial dependence on the wave vectors  $k$ . At late times these quantities approach frequencies of oscillation which become harmonic in that domain.

The coefficients appearing in the power-law factors in Eqs. (16) are given by

$$\begin{aligned} \beta_1 = \beta_2 = \beta'_1 = \beta'_2 &= \frac{1}{54c_\infty^4} \left( 1 + 8\alpha^2 + 64\alpha^4 + 32\alpha^6 + \frac{4\alpha^2\Lambda^2}{C_\tau^3 c_\infty^4 k^2} \right), & \beta_3 = \beta'_3 + 1 &= -\frac{2}{3}(1 - \alpha^2), \\ \beta_4 = \beta'_4 + \frac{1}{3} &= \frac{2\alpha^2}{27c_\infty^4} \left( 1 - 16\alpha^2 - \frac{2\Lambda^2}{C_\tau^3 c_\infty^4 k^2} \right), & \beta_5 = \beta_6 &= \frac{1}{6}(1 + 2\alpha^2), \end{aligned} \quad (20)$$

A key point which follows from these relations is the suppression of modes with large  $k$  relative to modes with smaller values of  $k$ . This fact was already noted in the numerical solutions discussed in Sec. III B (see also Fig. 2), but the asymptotic formulas Eqs. (16) in conjunction with Eq. (20) reveal the precise form of this suppression. Note also that the solution labeled by  $i = 3$  reproduces the transseries solution describing the homogeneous background, given by Eqs. (8) and (22) (with the integration constant independent of  $k$  in that case).

This highly nontrivial structure very accurately reproduces the behavior seen in the numerical calculations described in Sec. III B. At late time, the dominant asymptotic solutions for  $\delta\hat{T}$  and  $\delta\hat{\theta}$  are those which are least damped, i.e. those with the smallest value of  $A_i$ . For the  $\mathcal{N} = 4$

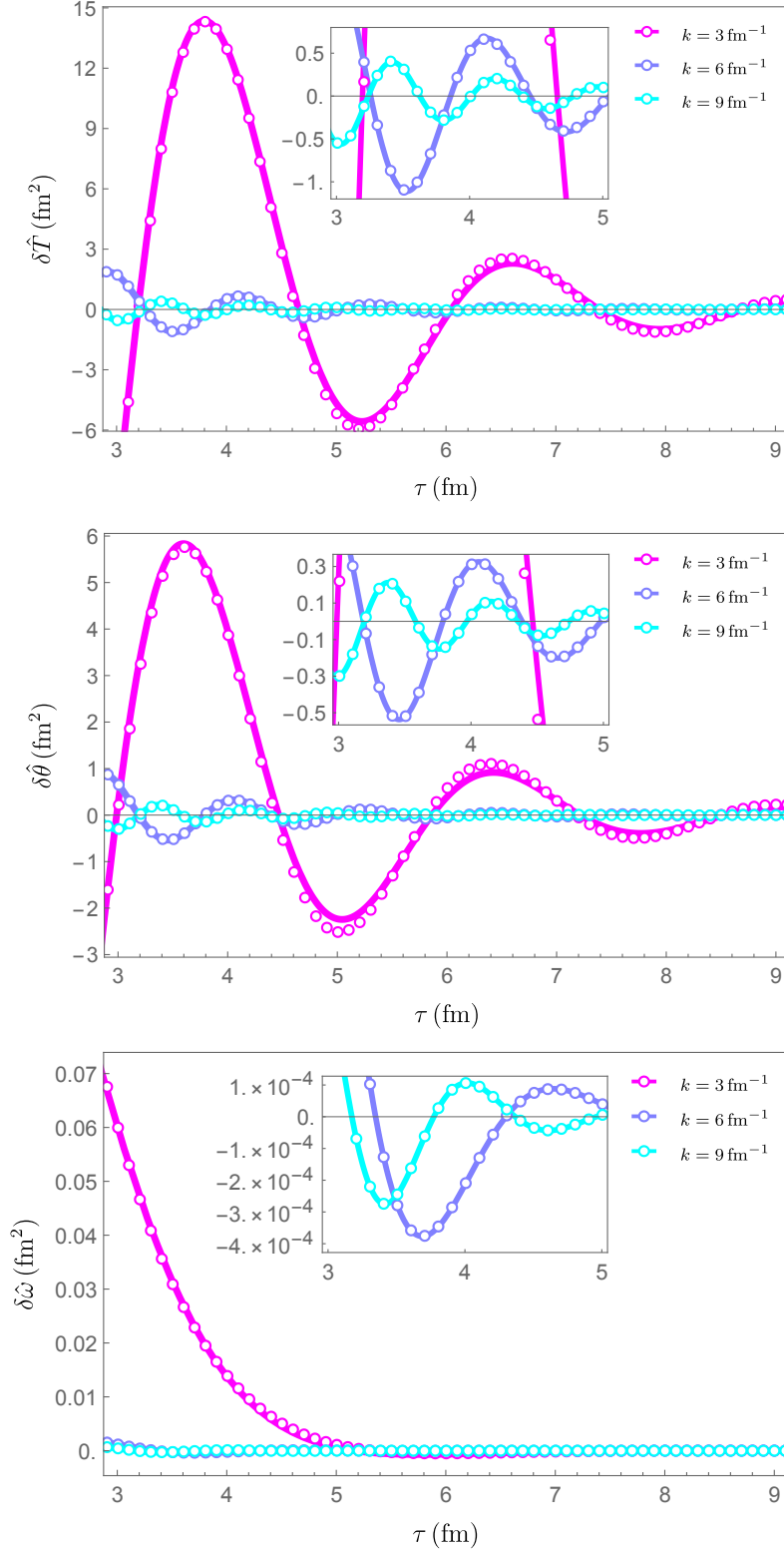


FIG. 3. The figures show the analytic late-time asymptotic solutions (solid lines) and the numerical results obtained in Sec. III A (discrete points) for various values of wave vector  $k$ . The inset plots are provided to give a better view of the small- $\tau$  region. The agreement is better for higher values of  $k$ ; at low values one could nevertheless improve it by incorporating subleading terms in Eq. (16).

supersymmetric Yang-Mills theory these are terms labeled by  $i = 1, 2$  in the solutions of Eqs. (16). These formulas then capture only the leading exponential behavior, but still give an excellent account of the numerical solutions, as illustrated in Fig. 3, especially for large and moderate values of the wave vector  $k$ . These plots were obtained by matching the complex amplitude  $C_1$  to initial data; the amplitude  $C_2$  is determined by conjugation, since the solutions are real. It is also quite interesting to compare these results with the asymptotics of Navier-Stokes theory, as well as with the case of ideal fluids. This is discussed in Appendix B.

The asymptotic solution discussed above applies to modes with  $k \neq 0$ . We now turn to the  $k = 0$  modes, which describe perturbations homogeneous in the transverse space. It is more convenient to study this case using Eqs. (13) which reduce to

$$\left(\partial_\tau + \frac{2\mathcal{A}}{9\tau}\right)\delta\hat{T} - \frac{1}{4\tau}\delta\hat{\pi}_i^i = 0, \quad (21a)$$

$$\left[(12 + \mathcal{A})\tau\partial_\tau - 4 + \frac{8C_\eta}{C_\tau} + \left(\frac{7}{3} - \frac{\tau T}{C_\tau}\right)\mathcal{A}\right]\delta u_i = 0, \quad (21b)$$

$$\frac{1}{9}(\tau T\mathcal{A} - 32C_\eta)\delta_{ij}\delta\hat{T} + \left(C_\tau\tau\partial_\tau + \tau T + \frac{2C_\tau\mathcal{A}}{9}\right)\delta\hat{\pi}_{ij} = 0. \quad (21c)$$

We observe that  $\delta u_i$  and  $\delta\hat{\pi}_{12}$  decouple from all other modes, and the only remaining coupling is between  $\delta\hat{T}$  and  $\delta\hat{\pi}_{ij}$ . The solutions in the late-time expansion are given by

$$\begin{aligned} \delta u_i(\tau) &\sim C_i(\Lambda\tau)^{\frac{1}{3}} \left(1 + 2\alpha^2 C_\tau(\Lambda\tau)^{-\frac{2}{3}} + \frac{4(1 + 6\alpha^2)\alpha^2 C_\tau^2}{9}(\Lambda\tau)^{-\frac{4}{3}} + \mathcal{O}((\Lambda\tau)^{-2})\right), \\ \delta\hat{T}(\tau) &\sim C_3 \left(1 + \frac{2\alpha^2 C_\tau}{3}(\Lambda\tau)^{-\frac{2}{3}} + \frac{4\alpha^2(1 + \alpha^2)C_\tau^2}{9}(\Lambda\tau)^{-\frac{4}{3}} + \mathcal{O}((\Lambda\tau)^{-2})\right) \\ &\quad + C_4(\Lambda\tau)^{-\frac{2}{3}(1-\alpha^2)} e^{-\frac{3}{2C_\tau}\tau^{\frac{2}{3}}} \left(1 + \mathcal{O}((\Lambda\tau)^{-\frac{2}{3}})\right), \\ \delta\hat{\pi}_{ii}(\tau) &\sim C_3 \frac{8\alpha^2 C_\tau}{3}(\Lambda\tau)^{-\frac{2}{3}} \left(1 + \frac{4(1 + 3\alpha^2)C_\tau}{9}(\Lambda\tau)^{-\frac{2}{3}} + \mathcal{O}((\Lambda\tau)^{-\frac{4}{3}})\right) \\ &\quad + \left(-C_4 \frac{2}{C_\tau} + C_5(-1)^i\right) (\Lambda\tau)^{\frac{2}{3}\alpha^2} e^{-\frac{3}{2C_\tau}(\Lambda\tau)^{\frac{2}{3}}} \left(1 + \mathcal{O}((\Lambda\tau)^{-\frac{2}{3}})\right), \\ \delta\hat{\pi}_{12}(\tau) &\sim C_6(\Lambda\tau)^{\frac{2}{3}\alpha^2} e^{-\frac{3}{2C_\tau}(\Lambda\tau)^{\frac{2}{3}}} \left(1 + \mathcal{O}((\Lambda\tau)^{-\frac{2}{3}})\right), \end{aligned} \quad (22)$$

where  $i = 1, 2$ . Note that  $\{C_n\}$  with  $n = 1, \dots, 6$  is another set of integration constants, distinct from those in Eqs. (16). The second solution in  $\delta\hat{T}$  is nothing but the transseries solution of  $T(\tau)$  in Eqs. (8) (and also the solution of  $\delta\hat{T}$  labeled by  $i = 3$  in Eqs. (16) if the integration constant is independent of  $k$ ). The above solutions also reproduce the transseries solution of  $\mathcal{A}(\tau)$  in Eqs. (8), using  $\delta\mathcal{A} = (9\delta\hat{\pi}_i^i - 8\mathcal{A}\delta\hat{T})/2$ .

To summarize, at late times the characteristics of the initial state are mapped to the scale  $\Lambda$  and dimensionless amplitudes  $\{C_n(k)\}$  which carry information about the structure of the initial data in the transverse plane. These numbers can be matched to a given numerical solution of Eqs. (15)

and (21). All physical observables that depend on the transverse dynamics can be expressed in terms of this asymptotic data, in manner described explicitly in the following section.

We now turn to the stability of the attractor in the presence of transverse perturbations. As seen in Eqs. (16) all nonzero modes are damped to zero at late times. The same is true for the zero-modes, with the exception of the velocity perturbations. As seen in Eq. (22), these grow as  $\delta u_i(\tau, \mathbf{k})|_{\mathbf{k}=0} \sim \tau^{1/3}$  at late times. This will invalidate the linear approximation at sufficiently late times, unless the initial condition for this mode is zero – in this special case it remains zero in the course of evolution, since (in contrast to nonzero modes) it is not sourced by other modes. If the initial amplitude is nonzero but small enough, the mild growth will not invalidate the linear approximation until after freeze-out. For applications to heavy-ion collision it is usually assumed that all modes of the velocity perturbation are negligible initially, which makes the picture described here workable.

It is interesting to note that the  $\tau^{1/3}$  behavior of the velocity zero-mode originates in the perfect-fluid theory, where it is easily seen to follow from energy-momentum conservation. It is likely that this is a general property of perturbations of Bjorken flow regardless of the dynamics. Further details concerning the perfect-fluid and NS limits are presented in Appendix B.

#### D. Spacetime evolution of QGP

We now turn to the problem of reconstructing the spacetime configuration at a given time from the evolved Fourier modes. The first step is the choice of background. This one wants to do in such a way as to be able to accommodate any initial condition relevant to heavy-ion physics. In this work we assume that the initial velocity perturbations vanish, along with the initial  $\delta\pi^{\mu\nu}$ . What remains is the initial condition for the energy density (or effective temperature) profile in the transverse plane.

Given an initial effective temperature profile  $T(\tau_i, \mathbf{x})$ , the first task is to determine a suitable Bjorken background, that is, the initial temperature  $T(\tau_i)$ . The initial condition is then split into two parts as required by Eq. (10): the homogeneous background and a perturbation

$$T(\tau_i, \mathbf{x}) = T(\tau_i) + \delta T(\tau_i, \mathbf{x}) = T(\tau_i)(1 + \delta\hat{T}(\tau_i, \mathbf{x})), \quad (23)$$

Since we linearize in the perturbation, the validity of the above separation formally requires

$$|\delta T(\tau_i, \mathbf{x})| \lesssim T(\tau_i) \quad \text{or} \quad |\delta\hat{T}(\tau_i, \mathbf{x})| \lesssim 1. \quad (24)$$

One can ensure that this is satisfied at the initial time by choosing the background temperature

$$T(\tau_i) = T_{\max}/2 \tag{25}$$

where  $T_{\max}$  is the maximum temperature at the initial time. With this choice,  $\delta\hat{T}(\tau_i, \mathbf{x})$  varies between  $-1$  and  $1$  when  $T(\tau_i, \mathbf{x})$  varies between  $0$  and  $T_{\max}$  in the transverse. Thus, given an initial temperature profile in the transverse plane, we can always pick the background such that our perturbation satisfies Eq. (24) at the initial time. This condition persists at later times due to the damped nature of the solutions. Thus our approach at least formally makes sense for any initial effective temperature profile.

Once the background is chosen, the Fourier transform of  $\delta\hat{T}(\tau_i, \mathbf{x})$  then provides initial conditions for the mode equations. Realistic initial conditions are in principle superpositions of infinitely many Fourier modes, but due to the strong damping of modes with high  $k$ , one can approximate the initial state by keeping only some finite number of low- $k$  modes. In practice, one needs to evaluate the initial conditions on a finite grid in the transverse plane, calculate the Fourier transform, evolve the modes by solving Eqs. (13) and then compute the inverse Fourier transform to reconstruct the spacetime history of the QGP. The problem can thus be described by a finite set of modes which encode the transverse structure of the initial state. The procedure can be made highly efficient by applying the Fast Fourier Transform (see e.g. Ref. [24]).

In our pilot study we consider a computational domain which is a 40 fm by 40 fm square region in the transverse plane, described by a regular grid of 100 by 100 points. A corresponding (conjugate) grid is then constructed in  $\mathbf{k}$ -space – this also introduces a cutoff on large  $k$ . We have implemented the steps outlined above for the case of very simple initial conditions which assume  $\delta T$  in the form of a Gaussian distribution in transverse coordinates with a specified impact parameter  $b$ . The remaining fields are taken to vanish at the initial time, which is a natural choice at least in the case of the transverse velocity perturbation. This leads to results shown in Fig. 4; they are analysed in more detail in Sec. IV. One can of course apply this approach to initial states generated in other ways, such as events generated using Glauber Monte-Carlo.

#### IV. QGP PHYSICS

In this section we would like to present some results which indicate that the set of approximations which we have adopted captures important physical effects which are beyond the scope of the Bjorken model. In particular, we describe some quantitative analysis of the numerical calculation described in Sec. III D. The numerical solutions (16) discussed in that section show that at asymptotically late times the modes representing the perturbations characterised by nonvanishing wavenumbers are damped away and eventually the system follows the Bjorken background solu-

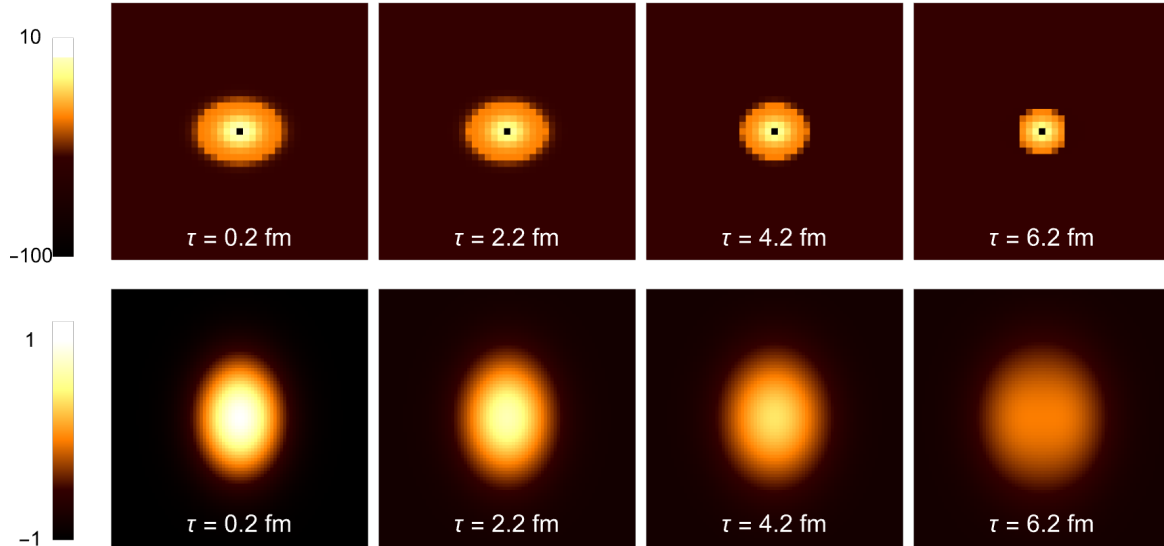


FIG. 4. The evolution of temperature profile in the transverse  $\mathbf{k}$ -space ( $\delta\hat{T}(\mathbf{k})$  with units  $\text{fm}^2$  in the top row) and  $\mathbf{x}$ -space (the dimensionless  $\delta\hat{T}(\mathbf{x})$  in the bottom row) at different instants of proper time. The initial conditions assume the nuclear radius of 6.62 fm (corresponding to lead). The impact parameter was taken to be  $b = 6$  fm. The dimensions of the region covered by the images are  $2 \text{ fm}^{-1}$  by  $2 \text{ fm}^{-1}$  in  $\mathbf{k}$ -space and 20 fm by 20 fm in  $\mathbf{x}$ -space.

tion. The QGP never reaches that stage, however due to hadronization: at some time the system described by the fluid is converted into a stream of particles. To calculate their distribution one needs to capture the fine details of the flow during the freeze-out epoch, when the hydrodynamic variables are converted into a set of outgoing hadrons over the freeze-out hypersurface  $\Sigma$ . This surface will be taken to be the locus where the local temperature drops below the transition temperature  $T_c \simeq 150 \text{ MeV}$ , estimated based on lattice calculations – we will not be distinguishing between chemical and kinetic freeze-out. Within the linearization framework discussed here, it is reasonable to model freeze-out at a single instant of proper time, determined by the homogeneous background via  $T(\tau_f) = T_c$ . In other words, the freeze-out hypersurface is taken to be both isothermal and isochronous, the difference between the two being beyond the linear approximation we consider here. To model the freeze-out surface under these assumptions we need to introduce its projection onto the transverse plane, denoted by  $\Sigma_\perp$ . Its boundary is determined by the condition that  $T(\tau_f, \mathbf{x}) = \sigma T_c$  (i.e.,  $\delta\hat{T}(\tau_f, \mathbf{x}) = \sigma - 1$ ), where  $\sigma$  is a model parameter which is principle could be fitted, but in this work we choose  $\sigma = 1/3$ . We have found that this leads to reasonable values of observables such as  $v_2$  and  $dN/dy$ . In the following, the area of the transverse plane projection of the freeze-out surface  $\Sigma_\perp$  is denoted by  $A_\perp$ .

The approximate determination of the freeze-out surface described above, as well the fact that the linearization is expected to work less well as the transverse flow builds up, suggests that one may not be able to obtain quantitative agreement with experimental data. We will however see



that at least some of the expected features, such as flow coefficients, can be calculated and are found to be of the expected order of magnitude.

### A. Multiplicity distributions

In heavy-ion collision experiments, momentum distributions of hadronized particles are given by the well-known Cooper–Frye formula [25]. We first consider the Bjorken background, with fluid velocity  $u^\mu = (\cosh \eta, \mathbf{0}, \sinh \eta)$ , where  $\eta$  is the pseudo-rapidity of the fluid. For a given particle species with mass  $m$  and momentum  $p^\mu = (m_\perp \cosh y, \mathbf{p}_\perp, m_\perp \sinh y)$ , where  $m_\perp = \sqrt{m^2 + \mathbf{p}_\perp^2}$ , and  $y$  is the kinematic rapidity of the particle, the momentum distribution of particles created on the freeze-out surface  $\Sigma$  is given by

$$\frac{dN_{\text{B}}(p_\perp)}{p_\perp dp_\perp d\phi dy} = \frac{1}{(2\pi)^3} \int_\Sigma d^3\sigma_\mu p^\mu f(x, p) = \frac{m_\perp \tau_f A_\perp}{(2\pi)^3} F_0. \quad (26)$$

Here

$$F_0(\tau_f, \hat{m}_\perp, \hat{p}_\perp) = 2K_1(\hat{m}_\perp) + \frac{1}{12} [\hat{p}_\perp^2 K_1(\hat{m}_\perp) - 2\hat{m}_\perp K_2(\hat{m}_\perp)] \mathcal{A}(\tau_f) \quad (27)$$

while  $\hat{p}_\perp \equiv p_\perp/T \equiv |\mathbf{p}_\perp|/T$ ,  $\hat{m}_\perp \equiv m_\perp/T$ ,  $d^3\sigma_\mu = (\cosh \eta, \mathbf{0}, -\sinh \eta) \tau_f d\eta d^2x$  is the area element of the freeze-out surface  $\Sigma$ ,  $f(x, p) = e^{u \cdot \hat{p}} (1 + \varepsilon_{\mu\nu} \hat{p}^\mu \hat{p}^\nu)$  is the nonequilibrium distribution for classical particles with  $\varepsilon_{\mu\nu} = \pi_{\mu\nu}/2(\mathcal{E} + p)$  being its viscous correction, and  $K_n(x)$  are Bessel functions of the second kind. Eq. (26) reduces to its NS limit [26] when higher order terms in  $\mathcal{A}$  are neglected. Note that  $A_\perp$  cannot be calculated using the background alone due to the homogeneity in the transverse plane. Thus,  $A_\perp$  in Eq. (26) is essentially a regulator and can only be calculated once the perturbations are included.

At large  $\hat{p}_\perp$ ,  $F_0 \sim \frac{\sqrt{2\pi}}{24} \mathcal{A} \hat{p}_\perp^{3/2} e^{-\hat{p}_\perp}$  (cf. the ideal limit where  $F_0 \sim \sqrt{2\pi} \hat{p}_\perp^{-1/2} e^{-\hat{p}_\perp}$ ) and thus Eq. (26) behaves like  $\hat{p}_\perp^{5/2} e^{-\hat{p}_\perp}$ . The ratio of the dissipative and ideal parts in Eq. (26) is asymptotically  $\mathcal{A} \hat{p}_\perp^2/24$ , which shows that the dissipative part is no longer subleading for sufficiently large  $p_\perp$ .

Taking into account corrections due to the perturbations up to quadratic order, the total multiplicity takes the form

$$\begin{aligned} \frac{dN(p_\perp, \phi)}{p_\perp dp_\perp d\phi dy} = \frac{m_\perp \tau_f A_\perp}{(2\pi)^3} & \left[ F_0 + F_1 \langle \delta \hat{T} \rangle_\perp + F_2 \hat{p}_\perp^i \langle \delta u_i \rangle_\perp + F_3 \hat{p}_\perp^i \hat{p}_\perp^j \langle \delta \hat{\pi}_{ij} \rangle_\perp + F_{11} \langle \delta \hat{T} \delta \hat{T} \rangle_\perp \right. \\ & \left. + F_{12} \hat{p}_\perp^i \langle \delta u_i \delta \hat{T} \rangle_\perp + F_{13} \hat{p}_\perp^i \hat{p}_\perp^j \langle \delta \hat{\pi}_{ij} \delta \hat{T} \rangle_\perp + F_{22} \hat{p}_\perp^i \hat{p}_\perp^j \langle \delta u_i \delta u_j \rangle_\perp + F_{23} \hat{p}_\perp^i \hat{p}_\perp^j \hat{p}_\perp^k \langle \delta \hat{\pi}_{ij} \delta u_k \rangle_\perp \right], \quad (28) \end{aligned}$$

where  $\hat{p}_{\perp 1} = \hat{p}_\perp \cos \phi$ ,  $\hat{p}_{\perp 2} = \hat{p}_\perp \sin \phi$  and  $\langle \dots \rangle_\perp = \int dx_1 dx_2 (\dots) / \int dx_1 dx_2$  denotes the spacial

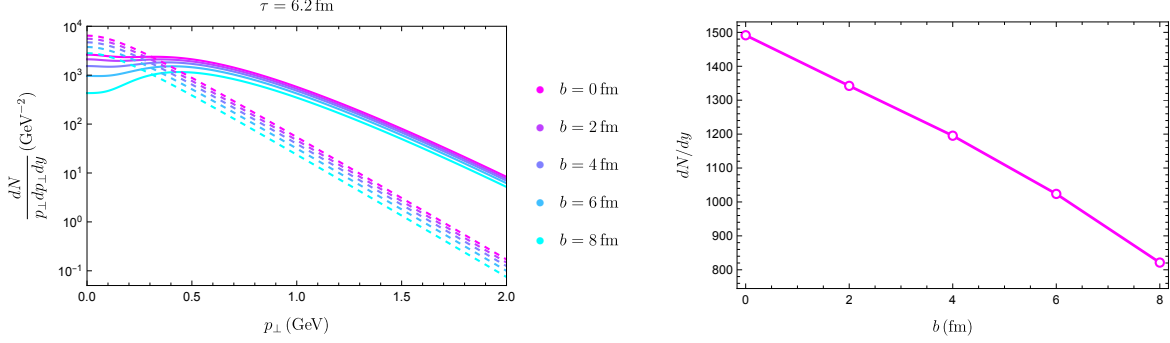


FIG. 5. This figure shows the dependence of multiplicity distribution on transverse momentum and impact parameter at freeze-out time  $\tau = 6.2$  fm. The left panel shows the transverse momentum dependence of  $\pi^{\pm}$  distribution without and with perturbations (represented by dashed and solid lines respectively). Although the relative contribution from perturbations is more significant compared to its background, its overall magnitude is negligibly smaller compared to the one in the lower  $p_{\perp}$  regime. The right panel shows the impact parameter (centrality) dependence of multiplicity for charged particles including pions, kaons and protons.

average over the projected freeze-out surface  $\Sigma_{\perp}$ . The functions  $F_1$ — $F_{23}$  are given by

$$\begin{aligned}
F_1 &= \hat{m}_{\perp} [K_0(\hat{m}_{\perp}) + K_2(\hat{m}_{\perp})] - \frac{1}{6} [(\hat{m}_{\perp}^3 + 3\hat{p}_{\perp}^2)K_1(\hat{m}_{\perp}) + 3\hat{m}_{\perp}(\hat{m}_{\perp} - 2)K_2(\hat{m}_{\perp})] \mathcal{A}, \\
F_2 &= 2F_{22} = F_0 = 2K_1(\hat{m}_{\perp}) + \frac{1}{12} [\hat{p}_{\perp}^2 K_1(\hat{m}_{\perp}) - 2\hat{m}_{\perp} K_2(\hat{m}_{\perp})] \mathcal{A}, \\
F_3 &= F_{23} = \frac{3}{4} K_1(\hat{m}_{\perp}), \\
F_{11} &= -\hat{m}_{\perp} K_0(\hat{m}_{\perp}) + \hat{m}_{\perp}^2 K_1(\hat{m}_{\perp}) + \frac{1}{24} [-14\hat{m}_{\perp}\hat{p}_{\perp}^2 K_0(\hat{m}_{\perp}) \\
&\quad + 2(14\hat{m}_{\perp}^2 + 42\hat{p}_{\perp}^2 + \hat{m}_{\perp}^2\hat{p}_{\perp}^2)K_1(\hat{m}_{\perp}) - (\hat{m}_{\perp}^3 + 12\hat{p}_{\perp}^2)K_2(\hat{m}_{\perp}) - \hat{m}_{\perp}^3 K_4(\hat{m}_{\perp})] \mathcal{A}, \\
F_{12} &= 2\hat{m}_{\perp} K_0(\hat{m}_{\perp}) \\
&\quad + \frac{1}{24} [\hat{m}_{\perp}(16 + \hat{p}_{\perp}^2)K_0(\hat{m}_{\perp}) + 2(16 - 2\hat{m}_{\perp}^2 - 7\hat{p}_{\perp}^2)K_1(\hat{m}_{\perp}) + \hat{m}_{\perp}\hat{p}_{\perp}^2 K_2(\hat{m}_{\perp})] \mathcal{A}, \\
F_{13} &= \frac{3}{4} [\hat{m}_{\perp} K_0(\hat{m}_{\perp}) - 5K_1(\hat{m}_{\perp})]. \tag{29}
\end{aligned}$$

In writing these equations we have suppressed the arguments of the functions  $F_i, F_{ij}$ . At a conceptual level, Eq. (28) shows explicitly that all the dependence on transverse dynamics is enters through the averages of the exponentially suppressed corrections to the homogeneous Bjorken background.

Integrating Eqs. (26) and (28) over  $\phi$  one finds

$$\frac{dN_B(p_{\perp})}{p_{\perp} dp_{\perp} dy} = \frac{m_{\perp} \tau_f A_{\perp}}{(2\pi)^2} F_0, \tag{30}$$

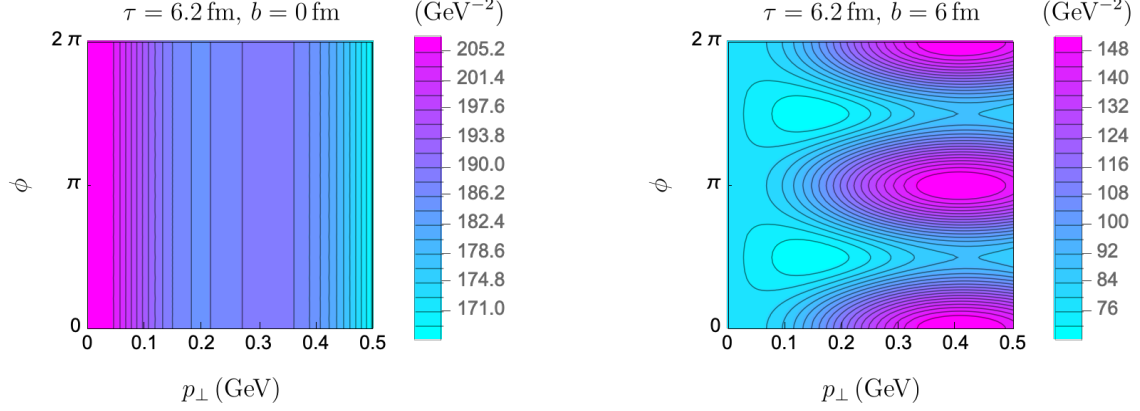


FIG. 6. This figure shows the 2D contour plot of the multiplicity distribution  $dN/p_{\perp} dp_{\perp} d\phi dy$  in  $(p_{\perp}, \phi)$  space at  $\tau = 6.2$  fm with different impact parameters, i.e.,  $b = 0$  fm (left) and  $b = 6$  fm (right) respectively.

and

$$\begin{aligned} \frac{dN(p_{\perp})}{p_{\perp} dp_{\perp} dy} = & \frac{m_{\perp} \tau_f A_{\perp}}{(2\pi)^2} \left[ F_0 + F_1 \langle \delta \hat{T} \rangle_{\perp} + F_{11} \langle \delta \hat{T} \delta \hat{T} \rangle_{\perp} \right. \\ & \left. + \frac{1}{2} \hat{p}_{\perp}^2 \left( F_3 \langle \delta \hat{\pi}_{ii} \rangle_{\perp} + F_{13} \langle \delta \hat{\pi}_{ii} \delta \hat{T} \rangle_{\perp} + F_{22} \langle \delta u_i \delta u_i \rangle_{\perp} \right) \right], \end{aligned} \quad (31)$$

which is proportional to the zeroth order flow coefficient introduced in the next subsection. At small  $\hat{p}_{\perp}$ , Eq. (31) only depends on the temperature perturbations. At large  $\hat{p}_{\perp}$ , Eq. (31) is asymptotically dominated by terms  $\langle \delta \hat{T} \delta \hat{T} \rangle_{\perp}$  and  $\langle \delta u_i \delta u_i \rangle_{\perp}$ , with coefficients  $F_{11} \sim F_{22} \hat{p}_{\perp}^2 \sim \frac{\sqrt{2\pi}}{24} \mathcal{A} \hat{p}_{\perp}^{7/2} e^{-\hat{p}_{\perp}}$ , so that Eq. (31) behaves as  $\hat{p}_{\perp}^{9/2} e^{-\hat{p}_{\perp}}$ . Thus, at large  $\hat{p}_{\perp}$  the contribution from the perturbations dominates the background contribution. Despite this, the magnitude of the multiplicity distribution in the large  $p_{\perp}$  regime is much smaller than at small  $p_{\perp}$ . The  $p_{\perp}$  distributions of the total particle number  $N$  given by Eqs. (30) and (31), as well as the  $p_{\perp}$ -integrated result of Eq. (31) are shown in Fig. 5.

The dependence of the multiplicity on both  $p_{\perp}$  and  $\phi$  is shown in Fig. 6. In particular, we compare the dependence of the multiplicity distribution on  $\phi$  for two different impact parameters  $b$ . The distribution resulting from a central collision ( $b = 0$ ) does not depend on  $\phi$ , as one would expect, due to the isotropy of the system. On the other hand, the right panel clearly shows the dependence on the azimuthal angle for a noncentral collision. This demonstrates the importance of the contribution from perturbations for both the magnitude of particle yields and of the angular distribution in the transverse plane.

## B. Collective flow

In order to study the collective behavior, it is convenient (and standard practice) to expand the multiplicity distribution geometrically in the transverse angle  $\phi$ . This expansion defines a series of flow harmonic coefficients  $v_n$ . The coefficients  $v_n(p_\perp)$  are defined via the differential form of the multiplicity distribution in  $p_\perp$ , i.e.,

$$\frac{dN(p_\perp, \phi)}{p_\perp dp_\perp d\phi dy} = v_0(p_\perp) \left( 1 + \sum_{n=1}^{\infty} 2v_n(p_\perp) \cos(n\phi) \right), \quad (32)$$

while the integrated ones are defined via the multiplicity distribution after its integration over  $p_\perp$ , i.e.,

$$\frac{dN(\phi)}{d\phi dy} = v_0 \left( 1 + \sum_{n=1}^{\infty} 2v_n \cos(n\phi) \right). \quad (33)$$

From Eq. (32) and Eq. (33), one finds

$$\begin{aligned} v_0(p_\perp) &= \int_0^{2\pi} \frac{dN(p_\perp, \phi)}{p_\perp dp_\perp d\phi dy} \frac{d\phi}{2\pi} = \frac{1}{2\pi} \frac{dN(p_\perp)}{p_\perp dp_\perp dy}, \\ v_0 &= \int_0^{2\pi} \frac{dN(\phi)}{d\phi dy} \frac{d\phi}{2\pi} = \frac{1}{2\pi} \frac{dN}{dy} = \int_0^\infty dp_\perp p_\perp v_0(p_\perp). \end{aligned} \quad (34)$$

That said,  $v_0(p_\perp)$  is the multiplicity averaged over the transverse angle  $\phi$ , while  $v_0$  is the total multiplicity  $dN/dy$ , up to a factor of  $1/2\pi$ . Anisotropy of the flow is reflected by the nonvanishing of the coefficients  $v_n$  for  $n > 0$ . From Eq. (32) and Eq. (33) one can also identify

$$\begin{aligned} v_n(p_\perp) &= \frac{1}{v_0(p_\perp)} \int_0^{2\pi} \frac{dN(p_\perp, \phi)}{p_\perp dp_\perp d\phi dy} \frac{d\phi}{2\pi} \cos(n\phi), \\ v_n &= \frac{1}{v_0} \int_0^{2\pi} \frac{dN(\phi)}{d\phi dy} \frac{d\phi}{2\pi} \cos(n\phi) = \frac{\int_0^\infty dp_\perp p_\perp v_0(p_\perp) v_n(p_\perp)}{\int_0^\infty dp_\perp p_\perp v_0(p_\perp)}. \end{aligned} \quad (35)$$

The last equality in Eq. (35) shows that the integrated coefficients  $v_n$  represent the averaged values of  $v_n(p_\perp)$  over the momentum spectrum.

In this paper we focus on the first few harmonic coefficients of  $v_n$  when  $n = 0, 1, 2$ , which describe the direct, radial, and elliptic flow respectively. Substituting Eq. (28) into Eq. (35), one

immediately finds

$$v_0(\hat{p}_\perp) = \frac{m_\perp \tau_f A_\perp}{(2\pi)^3} \left[ F_0 + F_1 \langle \delta \hat{T} \rangle_\perp + F_{11} \langle \delta \hat{T} \delta \hat{T} \rangle_\perp + \frac{1}{2} \hat{p}_\perp^2 \left( F_3 \langle \delta \hat{\pi}_{ii} \rangle_\perp + F_{13} \langle \delta \hat{T} \delta \hat{\pi}_{ii} \rangle_\perp + F_{22} \langle \delta u_i \delta u_i \rangle_\perp \right) \right], \quad (36a)$$

$$v_1(\hat{p}_\perp) = \frac{m_\perp \tau_f A_\perp \hat{p}_\perp}{2(2\pi)^3 v_0(\hat{p}_\perp)} \left[ F_2 \langle \delta u_1 \rangle_\perp + F_{12} \langle \delta \hat{T} \delta u_1 \rangle_\perp + \frac{1}{4} F_{23} \hat{p}_\perp^2 \left( \langle \delta u_1 (3\delta \hat{\pi}_{11} + \delta \hat{\pi}_{22}) \rangle_\perp + 2 \langle \delta u_2 \delta \hat{\pi}_{12} \rangle_\perp \right) \right], \quad (36b)$$

$$v_2(\hat{p}_\perp) = \frac{m_\perp \tau_f A_\perp \hat{p}_\perp^2}{4(2\pi)^3 v_0(\hat{p}_\perp)} \left[ F_3 \langle \delta \hat{\pi}_{11} - \delta \hat{\pi}_{22} \rangle_\perp + F_{13} \langle \delta \hat{T} (\delta \hat{\pi}_{11} - \delta \hat{\pi}_{22}) \rangle_\perp + F_{22} \langle \delta u_1^2 - \delta u_2^2 \rangle_\perp \right], \quad (36c)$$

where we suppressed the argument  $p_\perp$  of the coefficient functions  $F_i, F_{ij}$  given by Eq. (29). The asymptotic behavior of  $v_0(p_\perp)$ ,  $v_1(p_\perp)$ , and  $v_2(p_\perp)$  at small momentum is found to be

$$v_0(p_\perp) \sim 1, \quad v_1(p_\perp) \sim p_\perp, \quad v_2(p_\perp) \sim p_\perp^2 \quad \text{as } \hat{p}_\perp \rightarrow 0, \quad (37a)$$

while at large momentum one has

$$v_0(p_\perp) \sim \hat{p}_\perp^{9/2} e^{-\hat{p}_\perp}, \quad v_1(p_\perp) \sim \hat{p}_\perp^{-1}, \quad v_2(p_\perp) \sim \frac{\langle \delta u_1^2 - \delta u_2^2 \rangle_\perp}{2(4 \langle \delta \hat{T} \delta \hat{T} \rangle_\perp + \langle \delta u_i \delta u_i \rangle_\perp)} \sim 1 \quad \text{as } \hat{p}_\perp \rightarrow \infty. \quad (37b)$$

The asymptotic behavior of  $v_0(p_\perp)$  has already been analyzed below Eq. (31) where we studied the  $\phi$ -integrated multiplicity which is related to  $v_0(p_\perp)$  via Eq. (34). We observe that higher-order flow harmonics grow faster than  $p_\perp$  for small  $p_\perp$  and decrease slower at large  $p_\perp$ . In particular, we find that  $v_2(p_\perp)$  increases quadratically at small  $p_\perp$ , and saturates at large  $p_\perp$ . The dependence of the elliptic flow on the transverse momentum for various collision centralities (impact parameters) is illustrated in Fig. 7. The direct flow  $v_1$ , on the other hand, vanishes due to the specific symmetric initial condition which we used, which means that in this case, on average, there is no preferred direction for particle emission.

The integrated coefficients  $v_n$  can be obtained using Eqs. (35) and (36). Focusing on  $v_2$  we find the following analytic expression

$$v_2 = \frac{T^3 \tau A_\perp}{v_0(2\pi)^3} \left\{ -\frac{3}{16} (\hat{m}^2 \mathcal{I}_{2,1} - \mathcal{I}_{4,1}) \langle \delta \hat{\pi}_{ii} \rangle_\perp - \frac{3}{16} [\hat{m}^2 (5\mathcal{I}_{2,1} - \mathcal{I}_{3,0}) - 5\mathcal{I}_{4,1} + \mathcal{I}_{5,0}] \langle \delta \hat{T} \delta \hat{\pi}_{ii} \rangle_\perp + \left[ \frac{1}{4} (-\hat{m}^2 \mathcal{I}_{2,1} + \mathcal{I}_{4,1}) + \frac{\mathcal{A}}{96} (\hat{m}^4 \mathcal{I}_{2,1} + 2\hat{m}^2 (\mathcal{I}_{3,2} - \mathcal{I}_{4,1}) - 2\mathcal{I}_{5,2} + \mathcal{I}_{6,1}) \right] \langle \delta u_i \delta u_i \rangle_\perp \right\} \quad (38a)$$

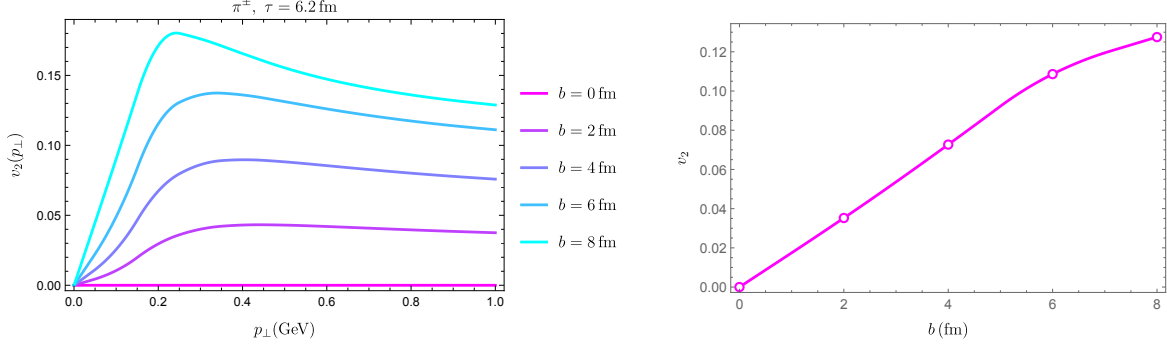


FIG. 7. This figure shows the dependence of elliptic flow on transverse momentum and impact parameter at freeze-out time  $\tau = 6.2$  fm. The left panel shows the dependence of differential  $v_2$  on transverse momentum for pions, while the right panel shows the dependence of the integrated  $v_2$  on impact parameter.

where

$$\begin{aligned}
v_0 = & \frac{T^3 \tau A_\perp}{(2\pi)^3} \left\{ 2\mathcal{I}_{2,1} - \frac{\mathcal{A}}{12} (\hat{m}^2 \mathcal{I}_{2,1} + 2\mathcal{I}_{3,2} - \mathcal{I}_{4,1}) \right. \\
& + \left[ \mathcal{I}_{3,0} + \mathcal{I}_{3,2} + \frac{\mathcal{A}}{6} (3\hat{m}^2 \mathcal{I}_{2,1} + 6\mathcal{I}_{3,2} - 3\mathcal{I}_{4,1} - 3\mathcal{I}_{4,2} - \mathcal{I}_{5,1}) \right] \langle \delta \hat{T} \rangle_\perp \\
& - \frac{3}{8} (\hat{m}^2 \mathcal{I}_{2,1} - \mathcal{I}_{4,1}) \langle \delta \hat{\pi}_{ii} \rangle_\perp - \frac{3}{8} [\hat{m}^2 (5\mathcal{I}_{2,1} - \mathcal{I}_{3,0}) - 5\mathcal{I}_{4,1} + \mathcal{I}_{5,0}] \langle \delta \hat{T} \delta \hat{\pi}_{ii} \rangle_\perp \\
& \quad - \left[ \mathcal{I}_{3,0} - \mathcal{I}_{4,1} \right. \\
& + \frac{\mathcal{A}}{24} (2\hat{m}^2 (42\mathcal{I}_{2,1} - 6\mathcal{I}_{2,2} - 7\mathcal{I}_{3,0} + \mathcal{I}_{4,1}) - 112\mathcal{I}_{4,1} + 12\mathcal{I}_{4,2} + 14\mathcal{I}_{5,0} + \mathcal{I}_{5,2} + \mathcal{I}_{5,4} - 2\mathcal{I}_{6,1}) \left. \right] \langle \delta \hat{T}^2 \rangle_\perp \\
& \quad \left. + \left[ \frac{1}{2} (-\hat{m}^2 \mathcal{I}_{2,1} + \mathcal{I}_{4,1}) + \frac{\mathcal{A}}{48} (\hat{m}^4 \mathcal{I}_{2,1} + 2\hat{m}^2 (\mathcal{I}_{3,2} - \mathcal{I}_{4,1}) - 2\mathcal{I}_{5,2} + \mathcal{I}_{6,1}) \right] \langle \delta u_i \delta u_i \rangle_\perp \right\}. \quad (38b)
\end{aligned}$$

The functions  $\mathcal{I}_{\ell,n}(\hat{m})$  are integrals defined in Appendix C, where they are expressed in terms of known special functions.

## V. SUMMARY AND OUTLOOK

Despite the radical simplifications made, the original Bjorken model of Ref. [1] provided a very useful analytic formula describing the dynamics of the energy density and has led to many important insights. The subsequent incorporation of viscous effects and higher orders in the large proper time expansion retained some of this simplicity, allowing for approximate analytic calculations and significantly simplifying numerical computations. However, the stringent symmetry requirements – boost invariance and homogeneity in the transverse plane – placed severe limits on how much of the physics could be described by such models. In this article our goal was to generalize the Bjorken model by incorporating the transverse dynamics in an approximate way so

as to capture physically crucial effects such as elliptic flow, which are inaccessible as long as all the symmetries of the Bjorken model are maintained. We have therefore partially relaxed these symmetry requirements, insisting only on longitudinal boost invariance while linearizing around a boost-invariant, transversely homogeneous attractor background, characterized only by a choice of the initial temperature. This approach aims to balance simplicity with the ability to capture more of the interesting physics of QGP. In this way we have formulated a description which goes beyond toy models, but still allows some analytic insights which can be extracted by applying asymptotic techniques.

The initial state is encoded in the initial conditions for the Fourier modes of the transverse perturbations and the initial temperature of the attractor background. The evolution equations map this information into a set of six exponentially suppressed scale-dependent amplitudes for each Fourier mode and the scale  $\Lambda$ . From the perspective of modern asymptotic analysis our work shows that the dynamics of QGP created in heavy-ion collision experiments provides a physical situation where the exponentially suppressed corrections to asymptotic power series solutions carry almost all the information which is actually detected in experiments. We have shown how these exponential corrections are translated into the physics post-freeze-out.

Aside from providing a clear, semianalytic picture of QGP evolution, our approach can be implemented numerically in a very straightforward and efficient fashion, since it relies on the discrete Fourier transforms and solving systems of coupled linear ODEs. The details of the initial state can be incorporated scale by scale in a controlled way: to account for finer details of the initial state, one can increase the number of modes used in the calculation. In this pilot study we have considered the build-up of elliptic flow and have found results qualitatively consistent with earlier work which relied on solving the fully-nonlinear problem (e.g. Ref. [14]). It is not clear how much quantitative agreement with actual experimental data can be achieved along these lines, one reason being that the applicability of linearization around the attractor is expected to deteriorate in the course of evolution due to the growth of transverse flow and may be somewhat rough by the time of freeze-out. It would be very interesting to better understand the limitations of our approach, identifying which physical effects are captured by this model, and which require a fully nonlinear treatment – an example of the latter may be turbulent phenomena [13].

Our approach, apart from its conceptual aspects, could also be used as a laboratory for studying models of the initial state, as well as novel characterizations of fluid behavior [27, 28]. Our model can also be extended in a number of ways; two most prominent are the description of jets [29–32], and the incorporation of noise [33–38]. We hope to return to these matters in the future.

## VI. ACKNOWLEDGMENTS

It is a pleasure to thank V. Ambrus, L. Du, W. Florkowski, S. Mrówczyński and M. Stephanov for helpful discussions. The authors would also like to thank the Isaac Newton Institute for Mathematical Sciences, Cambridge, for support and hospitality during the program “Applicable resurgent asymptotics: towards a universal theory” supported by EPSRC Grant No. EP/R014604/1. This work was supported by the National Science Centre, Poland, under Grant No. 2021/41/B/ST2/02909. For the purpose of Open Access, the authors have applied a CC-BY public copyright licence to any Author Accepted Manuscript (AAM) version arising from this submission.

## APPENDIX

### Appendix A: Linearized ODEs

The six first-order linear differential equations in Eqs. (15) can be written as three second-order linear differential equations by eliminating the variables  $\pi_{ij}$ , the resulting equations take the form

$$\partial_\tau^2 \delta \hat{T} + P_{TT}^{(1)} \partial_\tau \delta \hat{T}(\tau) + P_{T\theta}^{(1)} \partial_\tau \delta \hat{\theta} + P_{TT}^{(0)} \delta \hat{T} + P_{T\theta}^{(0)} \delta \hat{\theta} = 0, \quad (\text{A1a})$$

$$\partial_\tau^2 \delta \hat{\theta} + P_{\theta T}^{(1)} \partial_\tau \delta \hat{T} + P_{\theta\theta}^{(1)} \partial_\tau \delta \hat{\theta} + P_{\theta T}^{(0)} \delta \hat{T} + P_{\theta\theta}^{(0)} \delta \hat{\theta} = 0, \quad (\text{A1b})$$

$$\partial_\tau^2 \delta \hat{\omega} + P_{\omega\omega}^{(1)} \partial_\tau \delta \hat{\omega} + P_{\omega\omega}^{(0)} \delta \hat{\omega} = 0, \quad (\text{A1c})$$



with coefficients  $P_{AB}^{(n)}$ , where  $A, B = T, \theta, \omega$  and  $(n)$  denotes the differentiation order of the corresponding term:

$$\begin{aligned}
P_{TT}^{(1)} &= \frac{9(1+w) + 4\mathcal{A}}{9\tau}, \\
P_{T\theta}^{(1)} &= \frac{k(12 + \mathcal{A})}{36}, \\
P_{TT}^{(0)} &= \frac{-288\alpha^2 + (45w + 8\mathcal{A} + 36\tau\partial_\tau)\mathcal{A}}{162\tau^2}, \\
P_{T\theta}^{(0)} &= \frac{k}{324\tau} [36(3 + 2\alpha^2 + 3w) + (57 + 9w + 2\mathcal{A} + 9\tau\partial_\tau)\mathcal{A}], \\
P_{\theta T}^{(1)} &= \frac{12k}{12 + \mathcal{A}}, \\
P_{\theta\theta}^{(1)} &= P_{\omega\omega}^{(1)} = \frac{-36(1 - 2\alpha^2 - 3w) + (45 + 2\mathcal{A} + 9\tau\partial_\tau)\mathcal{A}}{9(12 + \mathcal{A})\tau}, \\
P_{\theta T}^{(0)} &= -\frac{k[12(8\alpha^2 + 3w) + (8 - 3w)\mathcal{A}]}{3(12 + \mathcal{A})\tau}, \\
P_{\theta\theta}^{(0)} &= \frac{1}{27(12 + \mathcal{A})\tau^2} \left\{ 108 [(1 - 2\alpha^2)(1 - w) + 4\alpha^2 k^2 \tau^2] + \left[ -\frac{3}{2}(58 - 32\alpha^2 - 6w + w\mathcal{A}) \right. \right. \\
&\quad \left. \left. + 36k^2 \tau^2 + (7 - 3w)(9w + 2\mathcal{A} + 9\tau\partial_\tau) \right] \mathcal{A} \right\}, \\
P_{\omega\omega}^{(1)} &= (7 - 3w)(9w + 2\mathcal{A} + 9\tau\partial_\tau)\mathcal{A}, \\
P_{\omega\omega}^{(0)} &= \frac{1}{27(12 + \mathcal{A})\tau^2} \left\{ 108 [(1 - 2\alpha^2)(1 - w) + 3\alpha^2 k^2 \tau^2] \right. \\
&\quad \left. + \left[ -\frac{3}{2}(58 - 32\alpha^2 - 6w + w\mathcal{A}) + (7 - 3w)(9w + 2\mathcal{A} + 9\tau\partial_\tau) \right] \mathcal{A} \right\}, \tag{A2}
\end{aligned}$$

where  $w \equiv \tau/\tau_\pi = \tau T/C_\tau$ . One immediately notices that the equation for vorticity  $\delta\hat{\omega}$  in Eqs. (A1) decouples from the other two equations. Given a solution to these equations, one can recover the independent shear-stress tensor components algebraically.

Substituting Eq. (5b) into Eqs. (A1), and taking the NS limit  $\tau_\pi \rightarrow 0$  (i.e.,  $C_\tau \rightarrow 0$ ), one obtains

$$\left( \partial_\tau + \frac{4C_\eta}{9\tau^2 T} \right) \delta\hat{T} + \frac{k}{3} \left( 1 + \frac{4C_\eta}{3\tau T} \right) \delta\hat{\theta} = 0, \tag{A3a}$$

$$-\frac{3(2C_\eta + \tau T)}{2C_\eta + 3\tau T} k \delta\hat{T} + \left( \partial_\tau + \frac{2C_\eta(7 + 6k^2\tau^2) - 3\tau T}{3\tau(2C_\eta + 3\tau T)} \right) \delta\hat{\theta} = 0, \tag{A3b}$$

$$\left( \partial_\tau + \frac{C_\eta(14 + 9k^2\tau^2) - 3\tau T}{3\tau(2C_\eta + 3\tau T)} \right) \delta\hat{\omega} = 0. \tag{A3c}$$

Note that in these equations  $T(\tau)$  is the background solution given explicitly in Eq. (5a). The above equations can also be obtained, by noting that in the NS limit the shear stress tensor perturbations  $\delta\hat{\pi}_{ij}$  are no longer independent degrees of freedom, and hence can be expressed in terms of the

hydrodynamic variables via

$$\delta\hat{\pi}_{ij}(\tau, \mathbf{k}) = \frac{1}{3} \left[ \delta_{ij} \delta\hat{T} + \left( \frac{1}{3} (\delta_{ij} - 3\hat{k}_i \hat{k}_j) \delta\hat{\theta}(\tau, \mathbf{k}) + \frac{1}{2} (\hat{k}_i \epsilon_{j\ell} + \hat{k}_j \epsilon_{i\ell}) \hat{k}^\ell \delta\hat{\omega}(\tau, \mathbf{k}) \right) k\tau \right] \mathcal{A}_{\text{NS}}(\tau), \quad (\text{A4})$$

which is resulted from Eq. (15d) by setting  $C_\tau = 0$  and  $\mathcal{A} = \mathcal{A}_{\text{NS}}$ . Substituting the above expression into Eqs. (15) and using again  $\mathcal{A} = \mathcal{A}_{\text{NS}}$ , one reproduces Eqs. (A3).

The ideal fluid equations are obtained simply by setting  $C_\eta = 0$  in Eqs. (A3).

We also note that Eq. (A3) can be approximated further in the late-time limit, when the timescale of the system is much larger than the typical microscopic timescale characterized by the shear viscosity:  $\tau \gg \tau_{\text{mic}} \sim \eta/(\mathcal{E} + p)$ , or equivalently  $C_\eta/\tau T \ll 1$ . In this case, Eqs. (A3) reduce to the equations studied in [13].

## Appendix B: The late-time asymptotic solutions in Navier-Stokes and ideal limits

The asymptotic solutions in the NS limit ( $C_\tau = 0$ ) can be obtained using Eqs. (A3). In the long-time limit  $\tau \rightarrow \infty$ , we find

$$\begin{aligned} \delta\hat{T}_{\text{NS}}(\tau) &\sim C_1 (\Lambda\tau)^{-\beta_4^{\text{NS}}} e^{-\frac{C_\eta k^2}{\Lambda^2} (\Lambda\tau)^{\frac{4}{3}} + \frac{3}{8C_\eta} (\Lambda\tau)^{\frac{2}{3}}} \left( 1 + \mathcal{O}((\Lambda\tau)^{-\frac{2}{3}}) \right) \\ &\quad + C_2 (\Lambda\tau)^{\beta_4^{\text{NS}}} e^{-\frac{3}{8C_\eta} (\Lambda\tau)^{\frac{2}{3}}} \left( 1 + \mathcal{O}((\Lambda\tau)^{-\frac{2}{3}}) \right), \end{aligned} \quad (\text{B1a})$$

$$\begin{aligned} \delta\hat{\theta}_{\text{NS}}(\tau) &\sim C_1 \frac{4C_\eta k}{\Lambda} (\Lambda\tau)^{-\beta_4^{\text{NS}} + \frac{1}{3}} e^{-\frac{C_\eta k^2}{\Lambda^2} (\Lambda\tau)^{\frac{4}{3}} + \frac{3}{8C_\eta} (\Lambda\tau)^{\frac{2}{3}}} \left( 1 + \mathcal{O}((\Lambda\tau)^{-\frac{2}{3}}) \right) \\ &\quad + C_2 \frac{3\Lambda}{4C_\eta k} (\Lambda\tau)^{\beta_4^{\text{NS}} - \frac{1}{3}} e^{-\frac{3}{8C_\eta} (\Lambda\tau)^{\frac{2}{3}}} \left( 1 + \mathcal{O}((\Lambda\tau)^{-\frac{2}{3}}) \right), \end{aligned} \quad (\text{B1b})$$

$$\delta\hat{\omega}_{\text{NS}}(\tau) \sim C_3 (\Lambda\tau)^{1/3} e^{-\frac{3C_\eta k^2}{4\Lambda^2} (\Lambda\tau)^{\frac{4}{3}}} \left( 1 + \frac{8C_\eta}{3} (\Lambda\tau)^{-2/3} + \mathcal{O}((\Lambda\tau)^{-\frac{4}{3}}) \right), \quad (\text{B1c})$$

where  $\beta_4^{\text{NS}} = -\frac{2}{3} - \frac{3\Lambda^2}{64C_\eta^3 k^2}$ . In the ideal limit,  $C_\tau = C_\eta = 0$ , from Eqs. (A3) one immediately obtains [13]

$$\delta\hat{T}_1(\tau) = (\Lambda\tau)^{1/6} \left( C_1 e^{-\frac{i}{\sqrt{3}} k\tau} + C_2 e^{\frac{i}{\sqrt{3}} k\tau} \right), \quad (\text{B2a})$$

$$\delta\hat{\theta}_1(\tau) = i\sqrt{3} (\Lambda\tau)^{1/6} \left( C_1 e^{-\frac{i}{\sqrt{3}} k\tau} - C_2 e^{\frac{i}{\sqrt{3}} k\tau} \right), \quad (\text{B2b})$$

$$\delta\hat{\omega}_1(\tau) = C_3 (\Lambda\tau)^{1/3}, \quad (\text{B2c})$$

where the coefficients  $\{C_n(k)\}$  are integration constants.

It is interesting to consider  $k = 0$  solutions in Eq. (22) in the NS limit  $C_\tau \rightarrow 0$  and compare

them to late-time solutions of the NS Eqs. (A3), which read

$$\begin{aligned}
\delta u_i^{\text{NS}}(\tau) &\sim C_i(\Lambda\tau)^{\frac{1}{3}} \left( 1 + \frac{8C_\eta}{3}(\Lambda\tau)^{-\frac{2}{3}} + \frac{32C_\eta^2}{9}(\Lambda\tau)^{-\frac{4}{3}} + \mathcal{O}((\Lambda\tau)^{-2}) \right), \\
\delta \hat{T}^{\text{NS}}(\tau) &\sim C_3 \left( 1 + \frac{2C_\eta}{3}(\Lambda\tau)^{-\frac{2}{3}} + \frac{4C_\eta^2}{9}(\Lambda\tau)^{-\frac{4}{3}} + \mathcal{O}((\Lambda\tau)^{-2}) \right), \\
\delta \hat{\pi}_{ii}^{\text{NS}}(\tau) &\sim C_3 \frac{8C_\eta}{3}(\Lambda\tau)^{-\frac{2}{3}} \left( 1 + \frac{4C_\eta}{3}(\Lambda\tau)^{-\frac{2}{3}} + \mathcal{O}((\Lambda\tau)^{-\frac{4}{3}}) \right), \quad \delta \hat{\pi}_{12}^{\text{NS}}(\tau) = 0.
\end{aligned} \tag{B3}$$

The exponential contributions to the solutions of  $\delta \hat{T}$  and  $\delta \hat{\pi}_{ij}$  in Eq. (22) vanish in this limit, the remaining asymptotic solutions are related via Eq. (A4). While the solution of  $\delta \hat{T}$  and  $\delta \hat{\pi}_{ij}$  coincides with the  $C_\tau \rightarrow 0$  limit of the MIS result in Eq. (22), the series for  $\delta u_i^{\text{NS}}$  deviates from the corresponding MIS result at subleading orders. This is a manifestation of the fact that the late-time expansion does not necessarily commute with the  $\tau_\pi \rightarrow 0$  limit.

The solution in the ideal limit can be obtained by taking  $C_\eta = 0$  in Eq. (B3). We note that the  $\tau^{1/3}$  growth of the  $k = 0$  velocity mode is a common feature shared by MIS, NS and perfect-fluid hydrodynamics. Indeed, one can see directly from the  $k = 0$  perfect-fluid equations that the decrease of the energy density caused by the longitudinal expansion along with the conservation of transverse momentum imply that the velocity perturbation must grow in a way which compensates the aforementioned fall-off of the background energy density. This suggests it is a feature of perturbations of flows satisfying the Bjorken symmetry assumptions and likely affects homogeneous perturbations of such flows regardless of the dynamics.

### Appendix C: Integrals for calculating elliptic flow

The functions  $\mathcal{I}_{\ell,n}(\hat{m})$  appearing in Eqs. (38) are defined by

$$\mathcal{I}_{\ell,n}(\hat{m}) \equiv \int_{\hat{m}}^{\infty} dx x^\ell K_n(x). \tag{C1}$$

This integration results from changing the integration variable from  $\hat{p}_\perp$  to  $x = \hat{m}_\perp = \sqrt{\hat{m}^2 + \hat{p}^2}$ , where  $\hat{m} \equiv m/T$ . The analytic expression of integrals what needed for calculating  $v_2$  are

$$\begin{aligned}
\mathcal{I}_{3,0} &= 4G_{1,3}^{3,0} \left( \begin{matrix} 1 \\ 0, 2, 2 \end{matrix} \middle| \frac{\hat{m}^2}{4} \right), & \mathcal{I}_{5,0} &= 16G_{1,3}^{3,0} \left( \begin{matrix} 1 \\ 0, 3, 3 \end{matrix} \middle| \frac{\hat{m}^2}{4} \right), & \mathcal{I}_{0,1} &= K_0(\hat{m}), \\
\mathcal{I}_{2,1} &= \hat{m}^2 K_2(\hat{m}), & \mathcal{I}_{4,1} &= 8G_{1,3}^{3,0} \left( \begin{matrix} 1 \\ 0, 2, 3 \end{matrix} \middle| \frac{\hat{m}^2}{4} \right), & \mathcal{I}_{6,1} &= 32G_{1,3}^{3,0} \left( \begin{matrix} 1 \\ 0, 3, 4 \end{matrix} \middle| \frac{\hat{m}^2}{4} \right), \\
\mathcal{I}_{5,1} &= -\frac{1}{5} \hat{m}^6 K_1(\hat{m}) {}_1F_2 \left( \begin{matrix} 1 \\ \frac{7}{2}, \frac{7}{2} \end{matrix} \middle| \frac{\hat{m}^2}{4} \right) - \hat{m}^5 K_0(\hat{m}) \left( {}_1F_2 \left( \begin{matrix} 1 \\ \frac{5}{2}, \frac{7}{2} \end{matrix} \middle| \frac{\hat{m}^2}{4} \right) - 1 \right) + \frac{45\pi}{2}, \\
\mathcal{I}_{3,2} &= \hat{m}^3 K_3(\hat{m}), & \mathcal{I}_{5,2} &= 16G_{1,3}^{3,0} \left( \begin{matrix} 1 \\ 0, 2, 4 \end{matrix} \middle| \frac{\hat{m}^2}{4} \right), & \mathcal{I}_{5,4} &= \hat{m}^5 K_5(\hat{m}), \\
\mathcal{I}_{2,2} &= -\frac{\hat{m}^5}{200} \left\{ 5 \left[ \partial_x {}_2F_3 \left( \begin{matrix} \frac{5}{2}, x \\ 1, 3, \frac{7}{2} \end{matrix} \middle| \frac{\hat{m}^2}{4} \right) \right]_{x=1} + {}_2F_3 \left( \begin{matrix} \frac{5}{2}, \frac{5}{2} \\ 3, \frac{7}{2}, \frac{7}{2} \end{matrix} \middle| \frac{\hat{m}^2}{4} \right) \right\} \\
&+ \frac{\hat{m}^5}{120} (3 \log \hat{m} + 3\gamma + 4 - \log 8) {}_1F_2 \left( \begin{matrix} \frac{5}{2} \\ 3, \frac{7}{2} \end{matrix} \middle| \frac{\hat{m}^2}{4} \right) + \frac{\hat{m}^3}{3} - \frac{4\hat{m}^2 I_1(\hat{m})}{3} - 4\hat{m} + 2\hat{m} I_0(\hat{m}) + \frac{3\pi}{2}, \\
\mathcal{I}_{4,2} &= -\frac{1}{392} \hat{m}^7 \left\{ 7 \partial_x \left[ {}_2F_3 \left( \begin{matrix} \frac{7}{2}, x \\ 1, 3, \frac{9}{2} \end{matrix} \middle| \frac{\hat{m}^2}{4} \right) \right]_{x=1} + {}_2F_3 \left( \begin{matrix} \frac{7}{2}, \frac{7}{2} \\ 3, \frac{9}{2}, \frac{9}{2} \end{matrix} \middle| \frac{\hat{m}^2}{4} \right) \right\} \\
&+ \frac{1}{840} \hat{m}^7 (15 \log \hat{m} + 15\gamma + 8 - 15 \log 2) {}_1F_2 \left( \begin{matrix} \frac{7}{2} \\ 3, \frac{9}{2} \end{matrix} \middle| \frac{\hat{m}^2}{4} \right) \\
&+ \frac{\hat{m}^5}{5} - \frac{8\hat{m}^4 I_1(\hat{m})}{15} - \frac{4\hat{m}^3}{3} + \frac{2\hat{m}^3 I_0(\hat{m})}{3} + \frac{15\pi}{2}, \tag{C2}
\end{aligned}$$

where several new special functions, in addition to the gamma function  $\Gamma(x)$  and the Bessel function of the second kind  $K_n(x)$  discussed above, are introduced:

$$G_{p,q}^{m,n} \left( \begin{matrix} \mathbf{a}_p \\ \mathbf{b}_q \end{matrix} \middle| z \right) = \frac{1}{2\pi i} \int_L \frac{\prod_{j=1}^n \Gamma(1 - a_j + s) \prod_{j=1}^m \Gamma(b_j - s)}{\prod_{j=n+1}^p \Gamma(a_j - s) \prod_{j=m+1}^q \Gamma(1 - b_j + s)} \tag{C3}$$

is the Meijer G-function represented in the Mellin–Barnes-type line integral and  $\mathbf{a}_p = (a_1, \dots, a_p)$ ,  $\mathbf{b}_p = (b_1, \dots, b_p)$ .

$${}_pF_q \left( \begin{matrix} \mathbf{a}_p \\ \mathbf{b}_q \end{matrix} \middle| z \right) = \sum_{n=0}^{\infty} \frac{(a_1)_n \dots (a_p)_n}{(b_1)_n \dots (b_q)_n} \frac{z^n}{n!}, \quad (a)_n = \frac{\Gamma(a+n)}{\Gamma(a)} = a(a+1)(a+2) \dots (a+n-1) \tag{C4}$$

is the generalized hypergeometric function.  $I_n(z)$  is the modified Bessel function of the first kind.

- 
- [1] J.D. Bjorken, *Highly Relativistic Nucleus-Nucleus Collisions: The Central Rapidity Region*, *Phys. Rev. D* **27** (1983) 140.
  - [2] M.P. Heller and M. Spaliński, *Hydrodynamics Beyond the Gradient Expansion: Resurgence and Resummation*, *Phys. Rev. Lett.* **115** (2015) 072501 [[1503.07514](#)].
  - [3] P. Romatschke, *Relativistic Fluid Dynamics Far From Local Equilibrium*, *Phys. Rev. Lett.* **120** (2018) 012301 [[1704.08699](#)].
  - [4] A. Kurkela, W. van der Schee, U.A. Wiedemann and B. Wu, *Early- and Late-Time Behavior of Attractors in Heavy-Ion Collisions*, *Phys. Rev. Lett.* **124** (2020) 102301 [[1907.08101](#)].
  - [5] J.-P. Blaizot and L. Yan, *Fluid dynamics of out of equilibrium boost invariant plasmas*, *Phys. Lett. B* **780** (2018) 283 [[1712.03856](#)].
  - [6] I. Muller, *Zum Paradoxon der Wärmeleitungstheorie*, *Z. Phys.* **198** (1967) 329.
  - [7] W. Israel, *Nonstationary irreversible thermodynamics: A Causal relativistic theory*, *Annals Phys.* **100** (1976) 310.
  - [8] R. Baier, P. Romatschke, D.T. Son, A.O. Starinets and M.A. Stephanov, *Relativistic viscous hydrodynamics, conformal invariance, and holography*, *J. High Energy Phys.* **04** (2008) 100 [[0712.2451](#)].
  - [9] M.P. Heller, A. Serantes, M. Spaliński and B. Withers, *Rigorous Bounds on Transport from Causality*, *Phys. Rev. Lett.* **130** (2023) 261601 [[2212.07434](#)].
  - [10] M. Spaliński, *Small systems and regulator dependence in relativistic hydrodynamics*, *Phys. Rev. D* **94** (2016) 085002 [[1607.06381](#)].
  - [11] W. Florkowski, M.P. Heller and M. Spaliński, *New theories of relativistic hydrodynamics in the LHC era*, *Rept. Prog. Phys.* **81** (2018) 046001 [[1707.02282](#)].
  - [12] J. Jankowski and M. Spaliński, *Hydrodynamic attractors in ultrarelativistic nuclear collisions*, *Prog. Part. Nucl. Phys.* **132** (2023) 104048 [[2303.09414](#)].
  - [13] S. Floerchinger and U.A. Wiedemann, *Fluctuations around Bjorken Flow and the onset of turbulent phenomena*, *JHEP* **11** (2011) 100 [[1108.5535](#)].
  - [14] M. Luzum and P. Romatschke, *Conformal Relativistic Viscous Hydrodynamics: Applications to RHIC results at  $s(NN)^{1/2} = 200$ -GeV*, *Phys. Rev. C* **78** (2008) 034915 [[0804.4015](#)].
  - [15] R.H. Price and J. Pullin, *Colliding black holes: The Close limit*, *Phys. Rev. Lett.* **72** (1994) 3297 [[gr-qc/9402039](#)].
  - [16] S. Bhattacharyya, V.E. Hubeny, S. Minwalla and M. Rangamani, *Nonlinear Fluid Dynamics from Gravity*, *J. High Energy Phys.* **02** (2008) 045 [[0712.2456](#)].
  - [17] A. Soloviev, *Hydrodynamic attractors in heavy ion collisions: a review*, *Eur. Phys. J. C* **82** (2022) 319 [[2109.15081](#)].
  - [18] M. Spaliński, *Initial State and Approach to Equilibrium*, *Acta Phys. Polon. Supp.* **16** (2023) 9 [[2209.13849](#)].
  - [19] I. Aniceto, D. Hasenbichler and A.O. Daalhuis, *The late to early time behaviour of an expanding plasma: hydrodynamisation from exponential asymptotics*, *J. Phys. A* **56** (2023) 195201 [[2207.02868](#)].

- [20] M.P. Heller, R. Jefferson, M. Spaliński and V. Svensson, *Hydrodynamic Attractors in Phase Space*, *Phys. Rev. Lett.* **125** (2020) 132301 [2003.07368].
- [21] I. Aniceto and M. Spaliński, *Resurgence in Extended Hydrodynamics*, *Phys. Rev. D* **93** (2016) 085008 [1511.06358].
- [22] C.M. Bender and S.A. Orszag, *Advanced Mathematical Methods for Scientists and Engineers*, McGraw-Hill (1978).
- [23] W. Wasow, *Asymptotic expansions for ordinary differential equations*, Pure and Applied Mathematics, Vol. XIV, Interscience Publishers John Wiley & Sons, Inc., New York-London-Sydney (1965).
- [24] W.H. Press, S.A. Teukolsky, W.T. Vetterling and B.P. Flannery, *Numerical Recipes in C*, Cambridge University Press, Cambridge, USA, second ed. (1992).
- [25] F. Cooper and G. Frye, *Single-particle distribution in the hydrodynamic and statistical thermodynamic models of multiparticle production*, *Phys. Rev. D* **10** (1974) 186.
- [26] D. Teaney, *The Effects of viscosity on spectra, elliptic flow, and HBT radii*, *Phys. Rev. C* **68** (2003) 034913 [nucl-th/0301099].
- [27] J.-Y. Ollitrault, *Measures of azimuthal anisotropy in high-energy collisions*, *Eur. Phys. J. A* **59** (2023) 236 [2308.11674].
- [28] V.E. Ambrus, S. Schlichting and C. Werthmann, *Establishing the Range of Applicability of Hydrodynamics in High-Energy Collisions*, *Phys. Rev. Lett.* **130** (2023) 152301 [2211.14356].
- [29] A.K. Chaudhuri and U. Heinz, *Effects of jet quenching on the hydrodynamical evolution of quark-gluon plasma*, *Phys. Rev. Lett.* **97** (2006) .
- [30] P.M. Chesler and L.G. Yaffe, *The Wake of a quark moving through a strongly-coupled plasma*, *Phys. Rev. Lett.* **99** (2007) 152001 [0706.0368].
- [31] J. Casalderrey-Solana, J.G. Milhano, D. Pablos, K. Rajagopal and X. Yao, *Jet Wake from Linearized Hydrodynamics*, *J. High Energy Phys.* **05** (2021) 230 [2010.01140].
- [32] Z. Yang, T. Luo, W. Chen, L. Pang and X.-N. Wang, *3d structure of jet-induced diffusion wake in an expanding quark-gluon plasma*, *Phys. Rev. Lett.* **130** (2023) .
- [33] Y. Akamatsu, A. Mazeliauskas and D. Teaney, *A kinetic regime of hydrodynamic fluctuations and long time tails for a Bjorken expansion*, *Phys. Rev. C* **95** (2017) 014909 [1606.07742].
- [34] X. An, G. Başar, M. Stephanov and H.-U. Yee, *Relativistic Hydrodynamic Fluctuations*, *Phys. Rev. C* **100** (2019) 024910 [1902.09517].
- [35] X. An, G. Başar, M. Stephanov and H.-U. Yee, *Fluctuation dynamics in a relativistic fluid with a critical point*, *Phys. Rev. C* **102** (2020) 034901 [1912.13456].
- [36] X. An, G. Başar, M. Stephanov and H.-U. Yee, *Evolution of non-gaussian hydrodynamic fluctuations*, *Phys. Rev. Lett.* **127** (2021) 072301 [2009.10742].
- [37] X. An, G. Başar, M. Stephanov and H.-U. Yee, *Non-Gaussian fluctuation dynamics in relativistic fluids*, *Phys. Rev. C* **108** (2023) 034910 [2212.14029].
- [38] Z. Chen, D. Teaney and L. Yan, *Hydrodynamic attractor of noisy plasmas*, *Phys. Rev. C* **108** (2023) 064911 [2206.12778].